

# Effects of Bound Diprotons and Enhanced Nuclear Reaction Rates on Stellar Evolution

Fred C. Adams<sup>a,b</sup>, Alex R. Howe<sup>c</sup>, Evan Grohs<sup>d</sup>, and George M. Fuller<sup>e</sup>

<sup>a</sup>*Physics Department, University of Michigan, Ann Arbor, MI 48109*

<sup>b</sup>*Astronomy Department, University of Michigan, Ann Arbor, MI 48109*

<sup>c</sup>*NASA Goddard Space Flight Center, 8800 Greenbelt Rd, Greenbelt, MD 20771*

<sup>d</sup>*Department of Physics, University of California Berkeley, Berkeley, California 94720*

<sup>e</sup>*Physics Department, University of California San Diego, La Jolla, CA 92093*

---

## Abstract

Deuterium represents the only bound isotope in the universe with atomic mass number  $A = 2$ . Motivated by the possibility of other universes, where the strong force could be stronger, this paper considers the effects of bound diprotons and dineutrons on stars. We find that the existence of additional stable nuclei with  $A = 2$  has relatively modest effects on the universe. Previous work indicates that Big Bang Nucleosynthesis (BBN) produces more deuterium, but does not lead to catastrophic heavy element production. This paper revisits BBN considerations and confirms that the universe is left with an ample supply of hydrogen and other light nuclei for typical cosmological parameters. Using the *MESA* numerical package, we carry out stellar evolution calculations for universes with stable diprotons, with nuclear cross sections enhanced by large factors  $X$ . This work focuses on  $X = 10^{15} - 10^{18}$ , but explores the wider range  $X = 10^{-3} - 10^{18}$ . For a given stellar mass, the presence of stable diprotons leads to somewhat brighter stars, with the radii and photospheric temperatures roughly comparable to those of red giants. The central temperature decreases from the characteristic value of  $T_c \approx 1.5 \times 10^7$  K for hydrogen burning down to the value of  $T_c \approx 10^6$  K characteristic of deuterium burning. The stellar lifetimes are smaller for a given mass, but with the extended possible mass range, the smallest stars live for trillions of years, far longer than the current cosmic age. Finally, the enhanced cross sections allow for small, partially degenerate objects with mass  $M_* = 1 - 10M_J$  to produce significant steady-state luminosity and thereby function as stars.

*Keywords:* Fine-tuning; Multiverse; Stellar Nucleosynthesis; Diprotons; Dineutrons

---

## 1. Introduction

The laws of physics, as realized in our universe, conspire to produce a long-lived expanding space-time that contains a wide range of astrophysical structures, from galaxy clusters down to small, rocky planets. An ongoing debate in cosmology considers whether our local universe is one out of many [1, 2, 3, 4, 5] and whether or not the laws of physics could be different in other (causally disconnected) regions. A related question is the degree to which the laws of physics are fine-tuned for the formation of astrophysical structures and ultimately the development of observers (see [6] for a recent review). A common example of possible fine-tuning concerns the bound state of the diproton (denoted here as  ${}^2p$ ). In our universe, deuterium is the only bound  $A = 2$  nucleus. If diprotons were bound and long-lived, then nuclear reactions could take place through the strong and electromagnetic interactions, without the weak force. The resulting cross sections could thus be larger by enormous factors,  $X$ , typically estimated as  $X \sim 10^{15} - 10^{18}$ .

Many authors (starting with [7]) claim that with such large cross sections, bound diprotons would have catastrophic consequences for the cosmos. One concern is that during the epoch of Big Bang Nucleosynthesis (BBN), all of the protons could be processed into helium, and perhaps heavier elements, leaving behind no hydrogen to produce water at later epochs. Similarly, in stellar interiors, the nuclear reaction rates could be so large that stars would have short lifetimes. Most authors make assertions of this nature by quoting earlier claims, but do not perform detailed calculations of either BBN or stellar evolution [8, 9, 10, 11, 12, 13, 14, 15], although some treatments are more nuanced [16, 17]. In contrast, recent work using a semi-analytic model for stellar structure [18, 19] indicates that a wide range of parameter space allows for stable, long-lived stars in universes with stable diprotons [20, 6]. Additional work finds that stable diprotons will not compromise BBN [21, 22], in that large mass fractions of hydrogen will remain. The first paper [21] also argues that diprotons will prevent the normal operations of stars, whereas the second [22] points out that diprotons produced during the BBN epoch can subsequently decay through the weak interaction and thereby produce large amounts of deuterium (which is still expected to be *more* stable). Similarly, bound dineutrons (denoted as  ${}^2n$ ) have only a modest effect on BBN yields [23], leading to a fractional change in the helium abundance of  $\sim 10\%$  (see also [24]). Notice also that BBN becomes ineffective in universes where the baryon to photon ratio  $\eta$  is smaller than that of our universe

[25, 26, 27]. The finding that BBN is only modestly affected by bound diprotons can be understood as follows. If the diproton is a bound state, then protons can interact through the strong force, with a greatly enhanced cross section. However, neutrons are present during BBN, so that  $n$ - $p$  reactions (which also do not require the weak interaction and have no coulomb barrier) are already dominant.

Given the contradictory claims in the previous literature, the goal of this paper is to revisit the previous BBN findings and to carry out detailed numerical simulations of stellar evolution for universes with stable diprotons. Here we use the publicly-available *MESA* code [28, 29]. This state-of-the-art numerical package is modified to include the greatly enhanced nuclear reaction cross sections arising due to stable diprotons and dineutrons.

In this paper, the key assumption is that diprotons are bound, but the cross sections and binding energies of other nuclei are only modestly affected. In our universe, dineutrons are unbound by an energy increment of order 100 keV, whereas diprotons have an additional Coulomb energy of order 500 keV [8]. Diprotons can become bound with an increase in the strong force coupling constant of order 10% [9, 13]. The main implication of bound diprotons is that nuclear reactions can take place without the weak force, so that the cross section for the first step of nucleosynthesis is greatly enhanced. The increased binding energy of diprotons would result in commensurate increases in the binding energy of other nuclei, but these changes are relatively small: In this context, the main nucleosynthesis product is helium, with binding energy 28.3 MeV, which could be increased by up to 10%. The additional energy available from the larger binding energy leads to somewhat longer stellar lifetimes. Since this effect is relatively small, and uncertain, this paper uses standard values for the binding energies of all nuclei except the diprotons and dineutrons. As a result, our estimates for stellar lifetimes should be considered as lower limits, where the true lifetimes are expected to be longer by a few percent.

This paper is organized as follows. Section 2 discusses the implications of bound diprotons on Big Bang Nucleosynthesis and finds that the light element abundances are only modestly affected. The reaction rates for stellar evolution, along with our approach to incorporating them, are then discussed in Section 3. The numerical results from the *MESA* simulations are presented in Section 4, including the modified main sequence, the time evolution of central temperature and luminosity, the mass-luminosity relationship, and the effects of varying the level of enhancement for the cross sections. The paper concludes in Section 5 with a summary of results and a discussion of their implications. For completeness, Appendix A presents the additional reactions arising for  $A = 2$  nuclei, with a focus on those relevant for BBN and stellar nucleosynthesis. Additional Appendices provide further detail concerning stellar evolution with bound diprotons, includ-

ing an explanation for the nearly constant photospheric temperatures seen in the simulations (Appendix B), a discussion of partially degenerate planetary mass “stars” (Appendix C), and the logarithmic dependence of the stellar lifetime on the nuclear enhancement factor (Appendix D).

## 2. Big Bang Nucleosynthesis Considerations

In this section we consider the ramifications of bound diprotons on BBN. If we suppose that a diproton is bound in our nuclear framework, then we can extend the scenario to include bound dineutrons. For a bound diproton, we estimate the Coulomb repulsion energy to be

$$V_{2p} = \frac{e^2}{4\pi r} \sim 0.36 \left( \frac{4 \text{ fm}}{r} \right) \text{ MeV}, \quad (1)$$

where  $r$  is the mean separation of the two nucleons. For the sake of definiteness, we consider values  $V_{2p} \simeq 0.5 \text{ MeV}$ , so that the binding energy of diprotons will be  $0.5 \text{ MeV}$  less than that of dineutrons. In addition, we will require the binding energy of diprotons to be small enough such that deuterium remains the most tightly bound (lowest energy)  $A = 2$  state. For purposes of estimating BBN effects in this section, we fix the diproton binding energy such that the beta decay reaction  ${}^2p \rightarrow d + e^+ + \nu_e$  is not energetically possible. As a result, diprotons have to capture leptons in order to transmute into deuterons.<sup>1</sup> For the diproton to deuteron reaction to be exothermic, we can relate the binding energy of the diproton to that of the deuteron,

$$B_{2p} < B_d - (m_n - m_p) \simeq 0.93 \text{ MeV}, \quad (2)$$

where  $m_n$  and  $m_p$  are the masses of the neutron and proton, respectively. To prevent diproton beta decays, we also require

$$B_{2p} > B_d - (m_n - m_p) - m_e \simeq 0.42 \text{ MeV}, \quad (3)$$

where  $m_e$  is the mass of the electron. We have ignored the mass of the neutrino in both of the above inequalities. With respect to the above considerations, we take the binding energies of the diproton and dineutron to be the following:

$$B_{2p} = 0.5 \text{ MeV} \quad \text{and} \quad B_{2n} = 1.0 \text{ MeV}. \quad (4)$$

---

<sup>1</sup>This assumption is made for simplicity. But even if diprotons can undergo beta decay, the lepton (mainly electron) capture reactions are still likely to be the dominant channel of transmutation. This also represents a relatively weakly bound diproton, which would be a smaller difference from our universe.

We preserve the deuteron binding energy at  $B_d = 2.2 \text{ MeV}$ .

All three dinucleon abundances will be in weak equilibrium with one another at sufficiently high temperatures. For  ${}^2p$  and  $d$ , we can calculate the abundance ratio with a Saha-like equation for the following weak interaction

$$e^- + {}^2p \longleftrightarrow d + \nu_e \quad \Rightarrow \quad \mu_e + \mu_{{}^2p} = \mu_d + \mu_{\nu_e}, \quad (5)$$

where  $\mu_i$  is the chemical potential of the relevant particle species  $i$ . Using Maxwell Boltzmann statistics for the baryonic states, we can calculate the abundance ratio of diprotons to deuterium,

$$\frac{Y_{{}^2p}}{Y_d} = \frac{g_{{}^2p}}{g_d} \exp \left[ \frac{B_{{}^2p} - B_d}{T} + \frac{m_n - m_p}{T} - \phi_e + \xi_{\nu_e} \right]. \quad (6)$$

There exists a similar expression for the dineutron to deuteron ratio

$$\frac{Y_{{}^2n}}{Y_d} = \frac{g_{{}^2n}}{g_d} \exp \left[ \frac{B_{{}^2n} - B_d}{T} - \frac{m_n - m_p}{T} + \phi_e - \xi_{\nu_e} \right]. \quad (7)$$

In equations (6) and (7),  $g_X$  are the spin degrees of freedom of nuclide  $X$ ,  $\phi_e = \mu_e/T$  is the electron degeneracy parameter, and  $\xi_{\nu_e} = \mu_{\nu_e}/T$  is the electron-neutrino degeneracy parameter. In writing both equations, we have assumed chemical equilibrium for a given lepton and anti-lepton. As the temperature decreases, the weak-interaction rates which govern the interconversion between free-neutrons and free-protons will fall out of equilibrium. In the standard cosmology, this process begins above a temperature of 1 MeV and persists until the formation of  ${}^4\text{He}$  below a temperature of 100 keV. In the presence of bound  ${}^2p$  and  ${}^2n$ , the free-neutron-to-free-proton ratio may maintain equilibrium to lower temperatures if the weak-interaction rates which govern the interconversion between the dinucleon states are fast. The neutron-to-proton interconversion would occur, e.g., via the following sequence

$$n(p, \gamma)d(e^+, \bar{\nu}_e){}^2p(\gamma, p)p. \quad (8)$$

For the above sequence to be an efficient pathway to weak equilibrium, the weak interaction and radiative capture/photo-dissociation reactions must all proceed rapidly. We will make the assumption that weak interactions such as  ${}^2p(e^-, \nu_e)d$  are slow on BBN time scales, but rapid on stellar evolution time scales. Therefore, the weak interactions for dinucleons will not maintain equilibrium for free neutrons and protons. However, for the small binding energies of the dinucleons, those abundances maintain Nuclear Statistical Equilibrium (NSE) down to low temperatures [30]. The abundance  $Y_X$  of nuclide  $X$  with atomic number  $Z$  and atomic mass number  $A$  is thus given by

$$Y_X = Y_p^Z Y_n^{A-Z} 2^{(A-3)/2} \pi^{3(A-1)/2} g_X A^{3/2} \left[ \frac{n_b}{(Tm_b)^{3/2}} \right]^{A-1} e^{B_X/T}, \quad (9)$$

where  $n_b$  is the baryon number density,  $T$  is the plasma temperature,  $m_b$  is the baryon rest mass, and  $B_X$  is the binding energy of nucleus  $X$ . The factor in square brackets represents the inverse of the entropy, so that the high entropy of the universe acts to keep the abundance  $Y_X$  low. The final exponential factor, due to nuclear binding, acts in the opposite direction. As a result,  $Y_X$  is determined by the competition between these opposing factors.

The abundances  $Y_p$  and  $Y_n$  of free protons and free neutrons will not follow weak equilibrium trajectories at low temperature in this model. As a result, they are free variables to be specified in equation (9). The resulting NSE ratios for the dinucleon abundances are thus given by

$$\frac{Y_{2p}}{Y_d} = \frac{Y_p g_{2p}}{Y_n g_d} e^{(B_{2p}-B_d)/T}, \quad (10)$$

and

$$\frac{Y_{2n}}{Y_d} = \frac{Y_n g_{2n}}{Y_p g_d} e^{(B_{2n}-B_d)/T}. \quad (11)$$

The deuteron is a spin-1 system, so that  $g_d = 3$ . The diproton and dineutron are both spin-0 systems, so that  $g_{2p} = g_{2n} = 1$ . Since the dineutron and diproton binding energies are less than that of the deuteron, the arguments in the above exponentials are strictly negative. If  $B_{2p} < B_{2n}$ , we would expect a larger abundance of dineutrons than diprotons. However, the diproton abundance is proportional to  $Y_p$ , instead of  $Y_n$  for the dineutron abundance, and this difference acts to enhance  $Y_{2p}$  over  $Y_{2n}$ . At early times ( $T > 10$  MeV), the neutron-to-proton ratio stays close to unity and the exponential suppression from the binding energy expression leads to  $Y_{2n} \gtrsim Y_{2p}$ . Conversely, at later times ( $T < 100$  keV), the neutron abundance becomes negligible, and it is possible for  $Y_{2p}$  and  $Y_{2n}$  to differ greatly.

For  $Y_{2p}$  and  $Y_{2n}$  to maintain NSE abundances, the rates of creation and destruction of the nuclei must be large. The radiative capture reactions  $p(p, \gamma)^2p$  and  $n(n, \gamma)^2n$  provide one channel for production and photo-dissociation. These channels are electromagnetic. The faster channels would be the following strong interactions with  $d$  in the final state

$$\begin{aligned} {}^2p(n, p)d & \quad N_A \langle \sigma v \rangle_{2pn} \sim 7 \times 10^8 \text{ cm}^3/\text{s}, \\ {}^2n(p, n)d & \quad N_A \langle \sigma v \rangle_{2np} \sim 7 \times 10^8 \text{ cm}^3/\text{s}, \end{aligned} \quad (12)$$

where  $N_A$  is Avogadro's number. For both reactions above, we have taken the thermally-averaged cross section from the reaction  ${}^3\text{He}(n, p)t$  to obtain an estimated strength. Once the reverse rates for the above two reactions fall below the Hubble expansion rate, diproton and dineutron synthesis will become inoperative. If there is a large abundance of free protons, an individual proton can capture on

${}^2n$  and destroy the  ${}^2n$  abundance. For  ${}^2p$ , if the free-neutron abundance is negligible, the main pathway for  ${}^2p$  transmutation would have to be a weak reaction or a photo-dissociation. Both pathways are temperature sensitive, so we would expect a freeze-out of the diproton abundance.

Our goal here is to estimate the dinucleon abundances at the point of departure from secular equilibrium. As a result, we need to determine the temperature at which the expressions in equations (10) and (11) no longer hold.

We begin by writing the Hubble expansion rate in terms of temperature for radiation-dominated conditions,

$$H = \sqrt{\frac{8\pi}{3} \frac{\pi^2}{30} g_\star} \frac{T^2}{m_{\text{pl}}} \simeq 1.3 \text{ s}^{-1} \left( \frac{g_\star}{43/4} \right) \left( \frac{T}{1 \text{ MeV}} \right)^2, \quad (13)$$

where  $g_\star$  is the statistical degrees of freedom of the radiation energy density, and  $m_{\text{pl}}$  is the Planck mass. The rate that keeps  ${}^2p$  in NSE is

$$\frac{dY_{2p}}{dt} = Y_d Y_p n_b \langle \sigma v \rangle_{2pn} e^{-Q_{2pn}/T}, \quad (14)$$

where  $Q_{2pn} = 1.7 \text{ MeV}$  is the  $Q$ -value for the  ${}^2p(n, p)d$  reaction. If we use the NSE ratio in equation (10), we can calculate the time-rate-of-change in the natural logarithm of  $Y_{2p}$ ,

$$\frac{d \ln Y_{2p}}{dt} = Y_n \frac{g_d}{g_{2p}} e^{(B_d - B_{2p})/T} \frac{2\zeta(3)}{\pi^2} T^3 \eta \langle \sigma v \rangle_{2pn} e^{-Q_{2pn}/T} = Y_n \frac{6\zeta(3)}{\pi^2} T^3 \eta \langle \sigma v \rangle_{2pn}. \quad (15)$$

Once the  ${}^2p$  production rate falls below the Hubble expansion rate,  $Y_{2p}$  no longer maintains NSE. Equating the rate  $d \ln Y_{2p}/dt$  to the Hubble expansion rate, we find

$$Y_n \frac{6\zeta(3)}{\pi^2} T^3 \eta \langle \sigma v \rangle_{2pn} = \sqrt{\frac{8\pi}{3} \frac{\pi^2}{30} g_\star} \frac{T^2}{m_{\text{pl}}}. \quad (16)$$

This expression can be solved for temperature to obtain

$$\begin{aligned} T &\simeq \sqrt{\frac{8\pi}{3} \frac{\pi^2}{30} \frac{\pi^2}{6\zeta(3)} \frac{1}{Y_n} \frac{1}{\eta \langle \sigma v \rangle_{2pn}} \frac{\sqrt{g_\star}}{m_{\text{pl}}}} \\ &\simeq 6 \times 10^{-9} \text{ MeV} \left( \frac{1}{Y_n} \right) \left( \frac{6 \times 10^{-10}}{\eta} \right) \left( \frac{1.16 \times 10^{-15} \text{ cm}^2}{\langle \sigma v \rangle_{2pn}} \right) \left( \frac{g_\star}{3.36} \right)^{1/2} \\ &\simeq 6 \times 10^{-2} \text{ MeV} \left( \frac{10^{-7}}{Y_n} \right) \left( \frac{6 \times 10^{-10}}{\eta} \right) \left( \frac{1.16 \times 10^{-15} \text{ cm}^2}{\langle \sigma v \rangle_{2pn}} \right) \left( \frac{g_\star}{3.36} \right)^{1/2}. \end{aligned} \quad (17)$$

The right-hand-side of equation (17) includes the neutron abundance, which is an implicit function of temperature. As a result, we caution that this expression should be taken only as a guide. For example, the first numerical expression is written in terms of the temperature where  $Y_{2p}$  freezes-out if  $Y_n = 1$ . Similarly, the second numerical expression gives the temperature where  $Y_{2p}$  freezes-out if  $Y_n = 10^{-7}$ . Figure 1 plots the evolution tracks of the various light nuclei mass fractions as a function of decreasing comoving temperature parameter,  $T_{\text{cm}}$ . The mass fraction is defined using the abundance

$$X_i = A_i Y_i, \quad (18)$$

for atomic mass number  $A_i$ , while  $T_{\text{cm}}$  is a proxy for the scale factor and differs from the plasma temperature due to heating of the plasma from electron-positron annihilation [31]. The solid lines are from an actual standard BBN calculation without bound diprotons or dineutrons [32]. The dotted lines give the mass fractions of diprotons and dineutrons assuming the secular equilibrium in equations (10) and (11). In addition, we plot the NSE mass fractions for the dinucleon states from equation (9). By inspection of Figure 1, we see that the value for the  ${}^2p$  freeze-out temperature for  $Y_n = 10^{-7}$  is an overestimate, while the value for  $Y_n = 1$  is a gross underestimate (using numerical values from equation [17]). However, if the diproton abundance follows the dotted curve from secular equilibrium, we see that the addition to the primordial deuterium abundance from diproton transmutation is small and of little consequence to the initial composition of stars at later epochs.

The dineutron abundance would follow a similar expression to the diproton abundance in equation (16), except for the replacement of the free-neutron abundance with the free-proton abundance. The proton abundance  $Y_p$  also has time dependence, but the mass fraction always stays close to unity in standard BBN as seen in Figure 1. As equation (17) indicates a low temperature for diproton freeze-out if  $Y_n = 1$ , we conjecture that the dineutron abundance would stay in secular equilibrium to very low temperatures. Therefore, we expect an insignificant addition to primordial deuterium from dineutron transmutation, as indicated by the dotted curves in Figure 1.

Our arguments in this section rely on a number of assumptions. First, we have used NSE and secular equilibria between the  $A = 2$  mass states to evolve the diproton and dineutron abundances. Figure 1 shows that all three of the  $A = 2$  mass fractions align with the NSE values down to a low temperature  $T \lesssim 100$  keV. However, immediately after the point of departure from NSE, the NSE values and actual/secular equilibrium values differ greatly. Second, both the NSE and secular equilibrium expressions are exponentially sensitive to binding energy. Picking different values of the diproton and dineutron binding energy will change

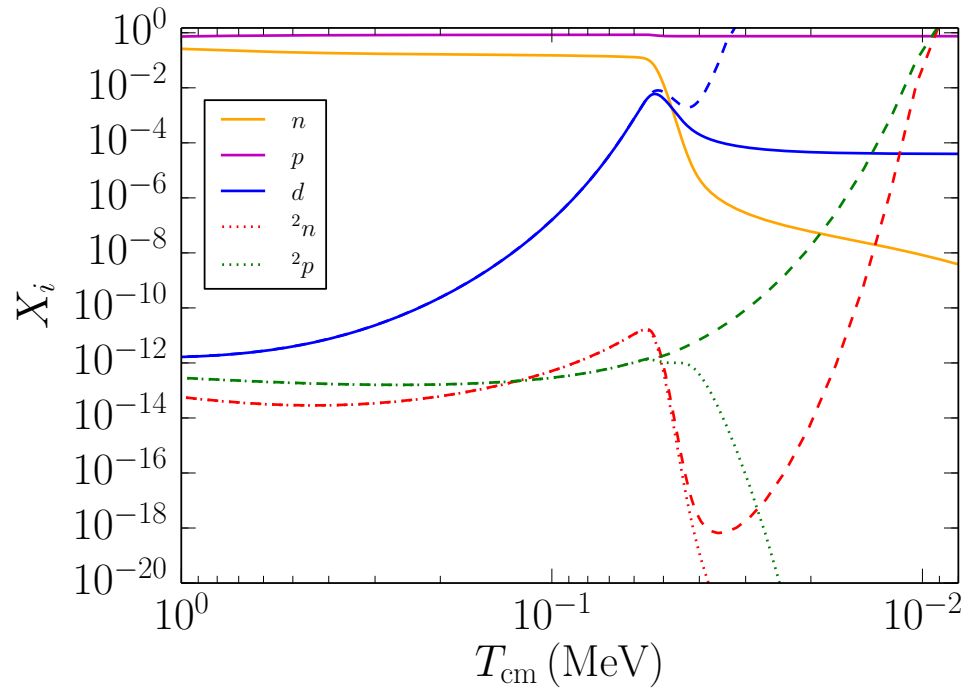


Figure 1: Standard BBN abundances (solid lines) as a function of decreasing  $T_{\text{cm}}$ . Dashed lines show NSE tracks for dinucleons (see equation [9]) and dotted lines show secular equilibrium tracks (see equations [10] and [11]).

the point of departure from NSE. Third, we used temperature-independent cross sections based on strong interactions for the  ${}^2p \leftrightarrow d \leftrightarrow {}^2n$  reactions. Introducing temperature dependence or changing the overall strength of the cross sections will also influence  $A = 2$  nucleosynthesis. Finally, we have only considered the reactions that create diprotons and dineutrons out of free particles or transmute them to deuterium. We have not considered other strong reactions, such as  $d({}^2n, n)t$ , which could lead to an earlier epoch of  ${}^4\text{He}$  synthesis and hence a larger primordial abundance.

Addressing the above criticisms requires a numerical calculation beyond our equilibrium estimates, as well as an extensive exploration of parameter space. Nevertheless, for the nuclear binding energies considered here, we estimate that the primordial abundance of free protons, deuterium, and helium will be approximately the same as from standard BBN in our universe. The high entropy of the universe prevents the conversion of most of the protons into bound states, as well as the construction of larger nuclei. The results from BBN could thus be different for universes in which the entropy is substantially lower.

### 3. Stellar Nuclear Reactions

This section considers the nuclear reactions that are relevant for stellar interiors. Only the reactions involving diprotons are significant. As shown above, BBN generally does not produce enough dineutrons to affect stellar evolution, and any dineutrons that are produced will have decayed into deuterium. The remaining reactions that affect the production of helium are discussed below.

The process starts with the original production reaction,



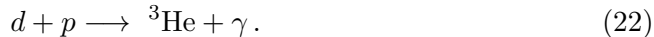
The weak decay of the diproton involves the production of a positron, which requires a minimum amount of energy (0.511 MeV). On the other hand, the center of the star contains a population of free electrons, so we expect the transformation reaction that turns diprotons into deuterium to be given by electron capture,



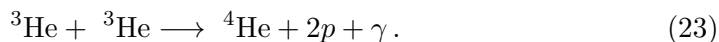
Although this reaction involves the weak force, it does not require the particles to overcome a Coulomb barrier, so the rate is much larger than the corresponding reaction at the start of the  $p$ - $p$  chain. Because the charges lead to an attractive force, the cross section is increased further due to the Sommerfeld enhancement. The remaining new reaction involves the interaction of the diproton with the deuteron to produce  ${}^3\text{He}$ ,



However, this new reaction is likely to be slower than the standard interaction of the deuteron, i.e.,



In the Sun, for example, the deuteron has a typical lifetime of about 4 seconds, which is much shorter than the typical interaction time of the original protons (a few Gyr). Moreover, the usual deuterium burning reaction (22) is likely to dominate over equation (21) because of the increased Coulomb repulsion in the latter. The resulting  ${}^3\text{He}$  then interacts through the usual channel,



This set of reactions corresponds to the so-called PPI chain in the Sun, where this channel accounts for about 85% of the helium production [33, 34, 35, 36]. For the cases of interest, we find that the operating temperature in stellar cores is lower (see Section 4) so that the suppression due to Coulomb barrier penetration is more severe, and the PPI chain should dominate over other channels by an even larger margin than in the Sun.<sup>2</sup> For completeness, we note that the presence of stable diprotons allows for the alternate reaction  ${}^3\text{He}({}^3\text{He}, {}^2p){}^4\text{He}$ , which produces a diproton instead of two separate protons. In our universe the original reaction (23) has a yield of 12.86 MeV, which is much larger than the binding energy of  ${}^2p$ , so that diproton production is expected to be minimal.

Given the above reactions, nuclear burning in stars containing stable diprotons could in principle proceed in different ways:

[II] In the first scenario, the production reaction (19) takes place, but the subsequent weak interaction (20) is slow. In this case, the star burns its protons into diprotons, but the diproton products remain inert (much like helium collects in stellar cores in our universe, but does not react until later stages of stellar evolution). The energy yield for this scenario is determined by the binding energy of the diproton. This binding energy is expected to be comparable to that of deuterium in our universe ( $B_d \approx 2.2$  MeV), about  $\sim 1$  MeV per particle.

[III] In the second scenario, the weak interaction (20) proceeds rapidly enough that diprotons are converted into deuterium as they are produced. The subsequent reaction (22) then produces  ${}^3\text{He}$ , in close analogy to the processes taking place in stellar cores in our universe, albeit with greatly enhanced cross sections. However, the temperature is generally too low for the  ${}^3\text{He}$  to be processed into  ${}^4\text{He}$  through equation (23). The stellar core is thus converted into  ${}^3\text{He}$ , but it burns in a later

---

<sup>2</sup>Recall that the CNO cycle is more temperature sensitive than the  $p$ - $p$  chain. The lower central temperatures for stars with diprotons thus results in a suppression of CNO reactions.

evolutionary stage. The binding energy of  ${}^3\text{He}$  is about 7.7 MeV in our universe, and is expected to be somewhat larger in a universe with stable diprotons. The energetic yield for this scenario is  $\sim 3$  MeV per particle.

[IIII] For some range of parameters, the nuclear burning temperature for the processes of equations (19 – 22) could be high enough that  ${}^3\text{He}$  is processed as it is synthesized. In this case, the original protons are transformed into  ${}^4\text{He}$  in a single stage of stellar nucleosynthesis, roughly analogous to the  $p$ - $p$  chain in the Sun. The energetic yield for this scenario is thus  $\sim 7$  MeV per particle (although the intermediate steps are different than for the standard  $p$ - $p$  chain).

Which of the scenarios is in play is determined by the relative rates of diproton destruction and production, where this ratio is given by

$$\mathcal{R} = \frac{n_e n_{2p} \langle \sigma v \rangle_{2pe}}{n_p^2 \langle \sigma v \rangle_{pp}} \approx \frac{n_{2p} \langle \sigma v \rangle_{2pe}}{n_p \langle \sigma v \rangle_{pp}}. \quad (24)$$

The following subsections estimate the diproton production cross section (denominator, Section 3.1) and the diproton destruction cross section (numerator, Section 3.2). These considerations indicate that the diproton destruction rate (via deuterium production) is fast enough to keep pace with diproton production, so that we expect  ${}^3\text{He}$  to be produced promptly through reactions (19), (20), and (22). On the other hand, the stellar evolution simulations of the following section indicate that the nuclear burning temperature is only  $T_c \sim 10^6$  K with the expected enhancement of the cross sections. This temperature is too low for  ${}^3\text{He}$  to react, so that  ${}^4\text{He}$  production takes place at a later epoch. As a result, stars are expected to follow scenario III.

### 3.1. Cross Section for Diproton Production

In general, the velocity averaged cross section for stellar nuclear reactions can be written in the form

$$\langle \sigma v \rangle = \left( \frac{8}{\pi m_R} \right)^{1/2} (kT)^{-3/2} \int \sigma E \exp[-kT/E] dE, \quad (25)$$

where  $m_R$  is the reduced mass of the two interacting particles [33, 35]. For charged particles undergoing non-resonant interactions, the cross section can be written as

$$\sigma(E) = \frac{S(E)}{E} \exp \left[ -(E_G/E)^{1/2} \right], \quad (26)$$

where  $E_G$  is the Gamow energy  $E_G = 2(\pi\alpha Z_1 Z_2)^2 m_R c^2$ . After integrating over the thermal distribution of particle energies, the resulting cross section (weighted

by velocity) can be written in the form

$$\langle\sigma v\rangle = \frac{8}{9} \left( \frac{2}{3E_G m_R} \right)^{1/2} \mathcal{S}_{\text{eff}} \Phi^2 \exp[-\Phi]. \quad (27)$$

where

$$\Phi \equiv 3(E_G/4kT)^{1/3}. \quad (28)$$

For  $p(p, e^+\nu)d$ ,  $m_R = m_p/2 = 469$  MeV and  $E_G = 493$  keV. If the reaction produces diprotons instead, the reduced mass and Gamow energy remain the same. The coefficient  $\mathcal{S}_{\text{eff}}$  is generally expressed in units of MeV-barn, where values for reactions of interest are given in Table 1. With this set of units of  $\mathcal{S}_{\text{eff}}$ , the cross section can be written in the form

$$\langle\sigma v\rangle = (1.43 \times 10^{-15} \text{cm}^3 \text{s}^{-1}) \mathcal{S}_{\text{eff}} \Phi^2 \exp[-\Phi]. \quad (29)$$

Finally, we can write the parameter  $\Phi$  in the form

$$\Phi = \lambda \Phi_0 \quad \text{where} \quad \lambda = (Z_1 Z_2)^{2/3} A^{1/3}, \quad (30)$$

where  $A = A_1 A_2 / (A_1 + A_2)$ . The value of  $\Phi_0$  is the same for all reactions (at a given temperature), i.e.,

$$\Phi_0 \approx 19.76 \left( \frac{T}{10^7 \text{K}} \right)^{-1/3}. \quad (31)$$

The expression for the cross section is then

$$\langle\sigma v\rangle = (1.43 \times 10^{-15} \text{cm}^3 \text{s}^{-1}) \mathcal{S}_{\text{eff}} \lambda^2 \Phi_0^2 \exp[-\lambda \Phi_0]. \quad (32)$$

In our universe, the cross section for the reaction  $p(d, \gamma)^3\text{He}$  is larger than that for  $p(p, e^+\nu)d$  by a factor  $X \approx 7 \times 10^{17}$  (see Table 1). As a first approximation, we expect a comparable enhancement factor for the reaction (19) that produces diprotons. However, the binding energy of  $^3\text{He}$  is (most likely) larger than that of the diproton, and nuclear reaction rates can vary by a few orders of magnitude even for analog reactions. For example, the cross section for  $t(p, \gamma)^4\text{He}$  is an order of magnitude smaller than that for the less energetic reaction  $d(p, \gamma)^3\text{He}$ . The  $p(p, \gamma)^2p$  reaction will be less energetic still, so we expect the cross section and enhancement factor to be smaller than the above estimate. For the sake of definiteness, this paper focuses on the values  $X = 10^{15}$  and  $X = 10^{18}$  for the stellar evolution calculations of the following section. Nonetheless, a wider range of enhancement factors is possible. It is useful to see how stellar evolution changes over a larger parameter space, so we also (briefly) consider stars with  $X = 10^{-3} - 10^{18}$  (see Section 4.4).

reaction	$\mathcal{S}_{\text{eff}}$ (MeV-barn)	$\lambda$	$X$
$pp \rightarrow d$	$3.36 \times 10^{-25}$	1	1
$pd \rightarrow {}^3\text{He}$	$2.50 \times 10^{-7}$	1.26	$7 \times 10^{17}$
$pp \rightarrow {}^2p$	$3 \times (10^{-10} - 10^{-7})$	1	$10^{15} - 10^{18}$

Table 1: **Cross Section Parameters**

For reactions that process protons into diprotons, the nuclear burning temperature is about  $T \sim 10^6$  K, so that  $\Phi_0 \approx 40$ . If we adopt enhancement factors in the range  $X = 10^{15} - 10^{18}$ , which corresponds to  $\mathcal{S}_{\text{eff}} \approx 3 \times 10^{-10} - 3 \times 10^{-7}$  MeV-barn, the resulting cross section from equation (32) can be estimated as

$$\langle \sigma v \rangle_{pp} \sim 3 \times (10^{-36} - 10^{-39}) \text{cm}^3 \text{s}^{-1}. \quad (33)$$

### 3.2. Weak Interaction Cross Section for Diproton Destruction

Weak interactions for stellar nucleosynthesis have been studied previously [37, 38]. Following this prior work, we define the quantity  $\langle ft \rangle$  such that the decay rate is given by

$$\Gamma = 1/\tau = \frac{\ln 2}{\langle ft \rangle} f, \quad (34)$$

where  $f$  is the phase space density factor. In approximate terms, the quantity  $\langle ft \rangle$  plays the role of the half-life divided by the phase space function. The matrix element for the interaction is given by

$$|M_{GT}|^2 = \sum_{if} \frac{n_p^i n_n^f}{2j_f + 1} |M_{GT}^{sp}|_{if}^2, \quad (35)$$

where the matrix element and the  $\langle ft \rangle$  factor are related through the approximate expression

$$\log_{10} \langle ft \rangle = 3.596 - \log_{10} |M_{GT}|^2. \quad (36)$$

After considerable analysis [37, 38], the cross section can be written in the form

$$\sigma = 2\pi^2 (\ln 2) \frac{\langle G \rangle}{\langle ft \rangle} \frac{(E + Q)^2}{m_e^5}, \quad (37)$$

where  $\langle G \rangle$  represents an integral over the phase space and is temperature dependent. Notice that  $\langle G \rangle$  is expected to be larger than unity due to the Sommerfeld

enhancement [39]. In this context, the operating temperature of the star ( $T_c \sim 10^6$  K) is low compared to the energy scales of interest ( $E \sim 1$  MeV  $\sim 10^{10}$  K), so that the expression can be evaluated in the low temperature limit. The quantity  $Q$  is the mass difference between the initial and final states. Here we are considering the capture process  ${}^2p(e^-, \nu_e)d$ , so that the initial mass is given by  $2m_p - B_{2p} + m_e$ , whereas the final mass is given by  $m_p + m_n - B_d$ . The difference determines the  $Q$  factor, which becomes

$$Q = m_p + m_e - m_n + B_d - B_{2p} \approx -0.8\text{MeV} + B_d - B_{2p}. \quad (38)$$

In order for the reaction to be energetically favored, the binding energy of deuterium must exceed the binding energy of the diproton by more than 0.8 MeV. In our universe, the  $B_d$  exceeds  $B_{2p}$  by more than 2.2 MeV, so if the binding energies increase together, diprotons can be transmuted into deuterons through reaction (20). For the particular choice  $B_{2p} = 0.5$  MeV (from Section 2), the factor becomes  $Q = 0.9$  MeV.

The time scale  $\langle ft \rangle / \langle G \rangle$  is determined by the weak interaction. As a working approximation, we expect this time scale to be comparable to the time  $\tau_n$  required for neutrons to decay. This latter time scale can be written in the form

$$\tau_n^{-1} = G_F^2 m_e^5 \mathcal{C}_1. \quad (39)$$

The dimensionless factor  $\mathcal{C}_1$  can be calculated from an effective field theory of the weak interaction where the quark degrees of freedom of the proton/neutron have been integrated out. In our universe,  $\mathcal{C}_1 = \lambda_0(1 + 3g_A^2)/2\pi^3$ , where the numerical factor  $\lambda_0 \approx 1.636$ , and  $g_A \approx 1.26$  is the axial-vector coupling factor for nucleons [40]. With this approximation, the cross section from equation (37) can be written in the form

$$\sigma = 2\pi^2 (\ln 2) \mathcal{C}_2 G_F^2 (E + Q)^2 \approx 2G_F^2 (E + Q)^2 \sim 4 \times 10^{-43} \text{cm}^2, \quad (40)$$

where the new dimensionless factor  $\mathcal{C}_2$  includes the nuclear physics relevant in the alternate universe where the strong force is stronger and diprotons are bound.<sup>3</sup> For the sake of definiteness, we have used  $\mathcal{C}_1 = \mathcal{C}_2$ , along with  $E + Q = 2$  MeV, to evaluate the cross section. The electron speed is given approximately by

$$v_e \approx \left( \frac{3kT}{m_e} \right)^{1/2} \approx 7 \times 10^8 \text{cm s}^{-1}, \quad (41)$$

---

<sup>3</sup>In general, if the strong force is altered, then the weak force is expected to change as well. Moreover, the axial-vector coupling  $g_A$  in our universe depends on the properties of nucleons, which can also change as the strong force is varied. However, we expect such changes to be modest.

so that we have

$$\langle\sigma v\rangle_{2pe} \sim 3 \times 10^{-34} \text{cm}^3 \text{s}^{-1}. \quad (42)$$

For the expected operating temperature of the star ( $T_c \sim 10^6$  K), this (velocity weighted) cross section is larger than that for producing diprotons by a factor of  $10^2 - 10^5$  over the expected range of nuclear enhancement factors  $X$  (see equation [33]). As a result, we expect diprotons to be converted into deuterium as fast as they are produced. As a working approximation, we can assume that the cross section for diprotons production corresponds to that for deuterium production. Moreover, as long as the  $e^-$  capture process is rapid compared to diproton production, the exact capture rate does not matter (the diprotons immediately capture electrons and become deuterium). Thus, the net result for stellar nucleosynthesis with stable diprotons is to make the factor  $\mathcal{S}_{\text{eff}}$  much larger than in our universe, where we consider enhancement factors in the range  $X = 10^{15} - 10^{18}$ .

The approximations outlined above should remain valid unless the weak interaction becomes significantly less effective than in our universe. However, if the rate at which electron capture converts diprotons into deuterium is too slow, then stars would process protons into diprotons, but the latter nuclei would remain inert. This alternate scenario is unlikely. Specifically, the dimensionless factor  $\mathcal{C}_2$  would have to be more than 100 times smaller than the value ( $\mathcal{C}_1$ ) in our universe, although it is expected to be *larger* due to Sommerfeld enhancement. To study this issue, future work should carry out a full Hartree-Fock type of calculation, which is beyond the scope of this present paper. Of course, even if diprotons cannot be rapidly converted into deuterium, stars would still operate, albeit with a lower yield. In this case, the energy produced per particle would be determined by the binding energy of the diproton instead of the (larger) binding energy of  ${}^3\text{He}$  (which holds when  $d + p \rightarrow {}^3\text{He}$  is rapid, as considered in this paper). This difference is a factor of  $\sim 3$  less energy yield per particle and would result in a commensurate decrease in stellar lifetimes.

#### 4. Results from Stellar Evolution Simulations

In this section, we present results obtained using the *MESA* stellar evolution code, a state of the art numerical package that is publically available [28]. Here we focus on scenario III, where electron capture is fast enough to convert diprotons into deuterium, but the  ${}^3\text{He}$  nuclei are not processed immediately.

To account for this scenario, we enhance the nuclear reaction rates for the  $p$ - $p$  chain by a constant factor  $X$ . In the usual  $p$ - $p$  chain, the first step is the production of deuterium through the fusion of two protons. This reaction is slow, due to the necessity of the weak interaction. In stars with stable diprotons, the

protons can fuse directly into diprotons through the strong interaction. The resulting diproton will then capture an electron and become deuterium as before (see equation [20]). Although this latter reaction still requires the weak interaction, it is much faster than usual  $p$ - $p$  reactions due to the absence of the coulomb barrier. In both scenarios, deuterium interacts rapidly with additional protons to become  ${}^3\text{He}$ . Since the latter interaction is fast, stellar evolution codes generally model the reaction as three protons producing  ${}^3\text{He}$ . The subsequent reactions involving the conversion of  ${}^3\text{He}$  to make  ${}^4\text{He}$  are then modeled explicitly. The net effect of having stable diprotons is thus to enhance the reaction rate for  ${}^3\text{He}$  production. The results of the previous section indicate that the enhancement factor is expected to be  $X \approx 10^{15} - 10^{18}$ . Here we focus on this range for  $X$ , but also explore a much wider range of values.

#### 4.1. The Main Sequence

For *MESA* simulations with nuclear enhancement factors  $X = 10^{15}$  and  $X = 10^{18}$ , Figure 2 shows the main sequence for stars with stable diprotons compared with those in our universe. For the standard main sequence in our universe, the stellar mass range is taken to be  $M_* = 0.08 - 100M_\odot$ . The upper mass cutoff is determined by stability considerations. For stars larger than about  $M_* \gtrsim 100 M_\odot$ , the pressure contribution due to radiation becomes larger than that due to thermal gas pressure, and the star becomes unstable [33, 34, 35]. This upper mass limit is independent of the source of the stellar luminosity and is expected to be the same for stars with stable diprotons. In addition, the mass-luminosity relation for sufficiently massive stars approaches the form  $L_* \sim 4\pi GcM_*/\kappa$ , where  $\kappa$  is the opacity. As a result, the brightest stars (with  $M_* = 100M_\odot$ ) have luminosity  $L_* \sim 10^6 L_\odot$ , as shown in Figure 2.

The lower mass cutoff is determined by the minimum mass capable of producing sustained nuclear fusion. This mass scale depends on the nuclear burning temperature, which in turn depends on the nuclear processes that power the star. For hydrogen burning stars in our universe, the lower mass cutoff is approximately  $M_* = 0.08 M_\odot$ . For stars with with stable diprotons and enhanced reaction cross sections, the nuclear burning temperature is lower, comparable to the deuterium burning temperature in our universe ( $T_c \sim 10^6$  K). With this value for the nuclear burning temperature, the minimum mass decreases down to  $M_* = 0.01 M_\odot = 10 M_J$ . As shown in Figure 2, the main sequence extends down to this mass scale. In addition, however, the numerical simulations show that nuclear burning can be sustained at even lower masses.

The resulting main sequence for stars with stable diprotons contains two distinct branches (see Figure 2). The upper branch corresponds to stars with masses in the range  $M_* = 0.01 - 100M_\odot$ , and displays a narrow range of photospheric

temperatures. The lower branch includes stars with masses in the range  $M_* = 0.5 - 10M_J$ , and displays a wider range of (much cooler) temperatures. These low-mass objects are primarily supported by electron degeneracy pressure and can thus be considered as the “degenerate branch” of the main sequence. In contrast, stellar objects on the upper main sequence are supported by thermal pressure, like ordinary stars in our universe.

More specifically, the upper branch of the main sequence is roughly similar to the main sequence for deuterium burning in our universe. This result is expected, as the large enhancement factors  $X$  for diproton reactions are motivated by the reaction cross sections for deuterium [26, 27]. The mass range for the upper main sequence is also consistent with that expected for deuterium burning. Moreover, the upper main sequence has a slowly varying photospheric temperature, nearly independent of stellar mass, with typical values in the range  $T_* \approx 3000 - 5000$  K. These photospheric temperatures not only span a narrower range (even though the mass range is larger for these diproton stars), but they are also cooler than ordinary hydrogen-burning stars. The slowly varying surface temperature leads to a different mass-luminosity relation, compared with stars in our universe (see Section 4.3 and Appendix B). The luminosity range for the upper main sequence is comparable to that of ordinary stars, and spans essentially the same nine orders of magnitude ( $L_* = 10^{-3} - 10^6 L_\odot$ ).

Figure 2 shows that the upper main sequence for both  $X = 10^{15}$  and  $X = 10^{18}$  are remarkably similar. Some uniformity is expected, because stellar properties depend only logarithmically on the enhancement factor  $X$  (Appendix D), but these main sequences are nearly identical. This result arises from the nearly constant surface temperatures for these stellar configurations. Because of the extreme temperature sensitivity of the opacity, photospheric temperatures cannot fall below a minimum value [41], so that the main sequence cannot move farther to the right in the diagram (for further discussion, see also Section 4.5 and Appendix C).

The lower branch of the main sequence shown in Figure 2 includes much smaller stars with masses comparable to Jupiter, i.e.,  $M_* = 0.5 - 10M_J$ . This collection of stellar objects spans an additional four orders of magnitude in luminosity and displays a wider range of photospheric temperature in spite of the smaller mass range. The minimum stellar mass for this lower branch is thus substantially smaller than the minimum mass for deuterium burning, i.e.,  $M_* \lesssim 0.5M_J$ . In this regime, the differences between stars with  $X = 10^{15}$  and  $X = 10^{18}$  are more pronounced, with the luminosities increasingly significantly with increasing enhancement factor (especially at the lowest stellar masses  $M_* \sim 1M_J$ ).

The two parts of the main sequence correspond to different types of stellar configurations. In the range  $M_* = 0.01 - 100M_\odot$ , the stars are supported primarily by thermal pressure, where the nuclear reactions provide heating for the gas that

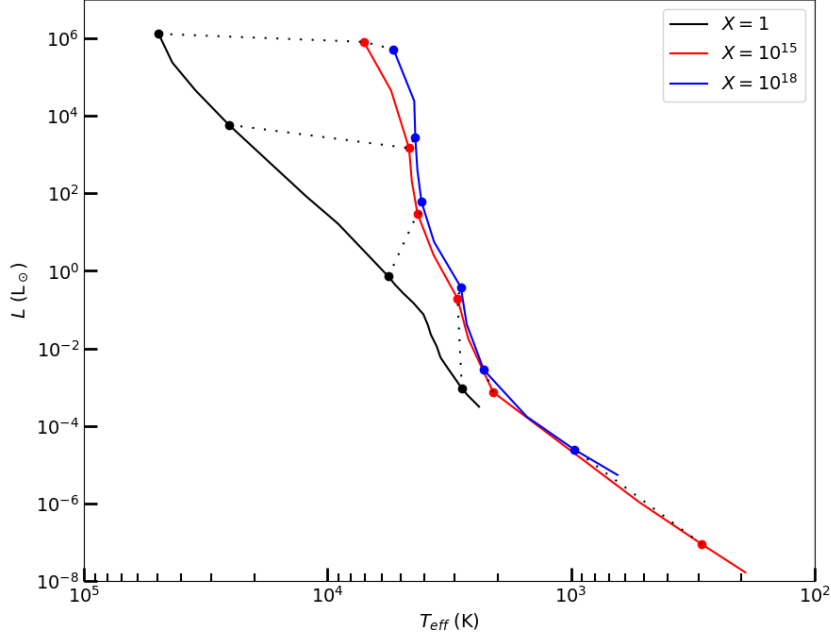


Figure 2: Main sequence for stellar nucleosynthesis in our universe (left black curve) and for universes with stable diprotons and enhanced nuclear reaction rates with  $X = 10^{15}$  (right red curve) and  $X = 10^{18}$  (right blue curve). The symbols denote specific stellar mass values:  $M_* = 100M_\odot$  (top),  $10M_\odot$ ,  $1M_\odot$ ,  $0.1M_\odot$  (bottom of black curve),  $10^{-2}M_\odot$ , and  $10^{-3}M_\odot = 1M_J$  (bottom of red curve). The standard main sequence extends down to  $M_* = 0.08M_\odot$ . The diproton main sequence contains two distinct branches (see text). For the upper branch with masses  $M_* = 0.01 - 100M_\odot$ , the main sequence is steep, with photospheric temperatures spanning a narrow range. For the lower branch with masses  $M_* < 0.01M_\odot = 10M_J$ , the stars have nearly constant radius, and the main sequence becomes less steep.

provides the pressure. These stars are thus like those in our universe. For the lower branch, with masses  $M_* < 0.01M_\odot$ , the main sequence slope corresponds to stellar configurations with nearly constant radius. This behavior indicates that the stars are supported primarily — but not entirely — by degeneracy pressure. These unusual objects are much like brown dwarfs in our universe, in that hydrostatic equilibrium does not rely on nuclear reactions, but here the greatly enhanced nuclear cross sections allow for substantial power generation (see Section 4.5 and Appendix C). For both branches of the main sequence, stars are able to achieve sustained nuclear power generation over time scales long enough to be of interest for cosmology and biology.

Figure 3 shows the internal structure of a star with mass  $M_* = 0.3M_\odot$  for enhanced nuclear reaction rates (solid curves) and for standard rates (dashed curves).

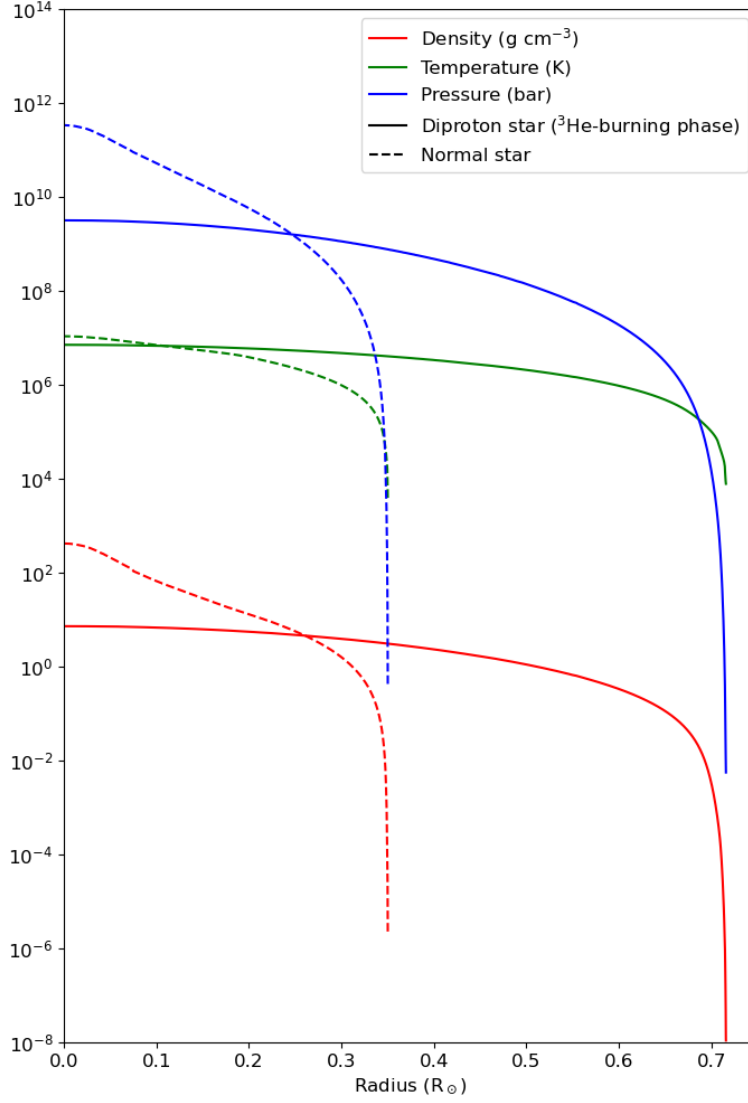


Figure 3: Comparison of stellar structure for stars with mass  $M_* = 0.3 M_\odot$  with standard nuclear reactions (dashed curves) and enhanced rates ( $X = 10^{15}$ , solid curves). The three sets of curves show the profiles for pressure (upper blue curves), temperature (middle green curves), and density (lower red curves) as a function of radial coordinate within the star.

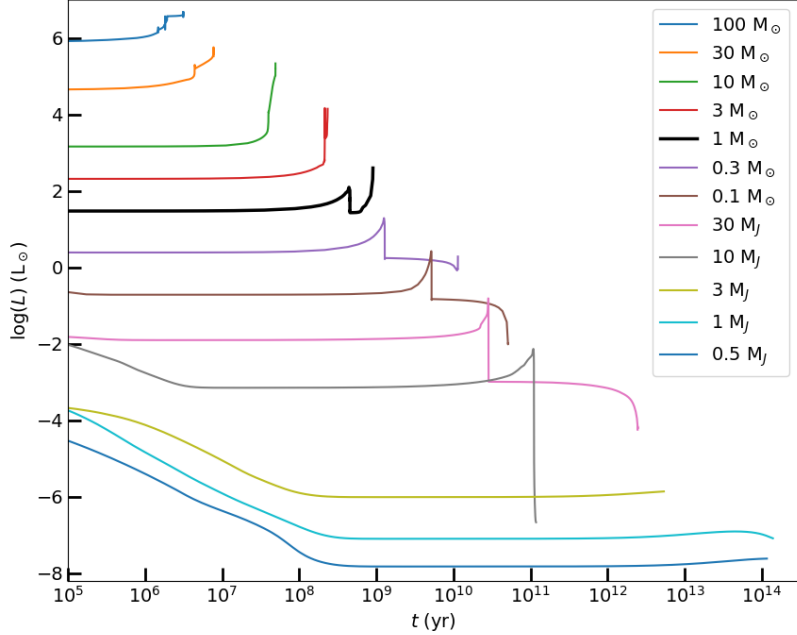


Figure 4: Stellar luminosity as a function of stellar age for stars with enhanced nuclear reaction rates  $X = 10^{15}$ .

This stellar mass was chosen because it represents one of the most common stars in our universe; moreover, its luminosity and lifespan in the alternate universe are roughly comparable to those of the Sun. The figure shows the profiles for pressure (blue curves), temperature (green curves), and density (red curves) for the two stars. For all three quantities, the central values are somewhat larger for the star with standard nuclear reactions rates and the profiles fall off more steeply. The star with enhanced reaction rates is about twice as large in radius and displays flatter profiles. The larger radius results in the cooler surface temperatures (redder colors) shown in the H-R diagram of Figure 2.

#### 4.2. Time Evolution of Stellar Properties

The stellar luminosity is shown as a function of stellar age in Figures 4 and 5, for enhancement factors  $X = 10^{15}$  and  $X = 10^{18}$ , respectively. All of the stars experience a short initial phase of declining brightness corresponding to pre-main-sequence contraction. This phase is relatively short, so that only the smallest stars show this behavior over the time scales shown in the figures. After this early transient phase, all of the stars experience an extended phase of nearly constant luminosity, corresponding to main-sequence nuclear reactions (protons  $\rightarrow$  diprotons  $\rightarrow$   ${}^3\text{He}$ ).

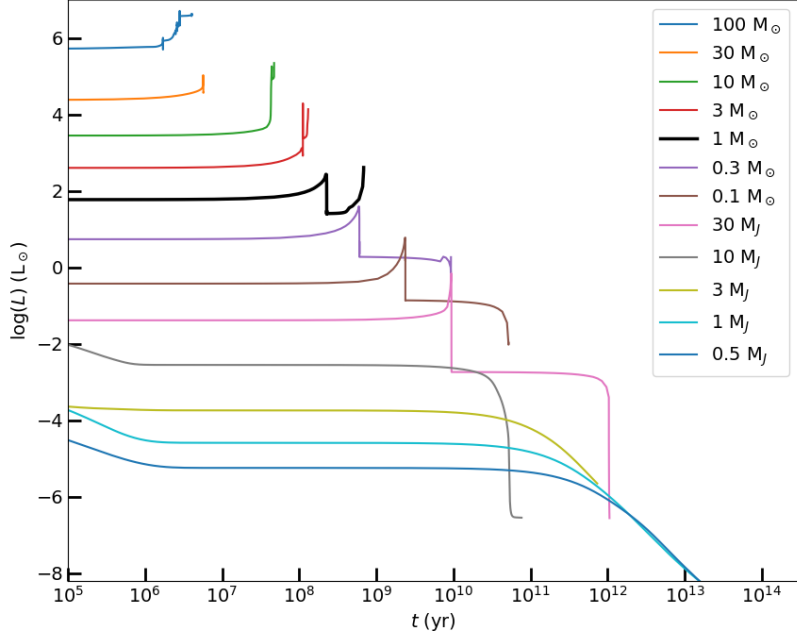


Figure 5: Stellar luminosity as a function of stellar age for stars with enhanced nuclear reaction rates  $X = 10^{18}$ .

For the lower mass stars, the central temperatures for burning protons into diprotons and then  ${}^3\text{He}$ , are relatively low, so that the latter species is not immediately processed into  ${}^4\text{He}$ . Instead, the lower mass stars display two distinct phases, first producing  ${}^3\text{He}$  as the product and then later transforming the  ${}^3\text{He}$  into  ${}^4\text{He}$ . These separate phases are evident in both Figures 4 and 5 for stars with masses in the range  $M_* = 0.03 - 1 M_\odot$ . For stars of even lower mass (specifically less than about  $M_* = 0.01 M_\odot = 10 M_J$ ), the central temperature cannot become high enough to burn  ${}^3\text{He}$ . These lowest-mass stars only experience the first of the two phases, and they end their lives with a  ${}^3\text{He}$  core. Higher mass stars with  $M_* > 1 M_\odot$  also have these two phases, but they are much shorter and more blended together as shown in the figures.

For the highest mass stars, the stellar lifetimes are comparable to those in our universe (millions of years). For solar type stars, the stellar lifetimes are shorter than those in our universe by about one order of magnitude, so that a star with

$M_* = 1M_\odot$  burns its hydrogen over  $\sim 1$  Gyr. In addition, we find that luminosity depends on stellar mass according to  $L_* \propto M_*^2$ , which represents a less steep dependence than that for ordinary hydrogen burning stars (where  $L_* \propto M_*^3$ ). As a result, the stellar lifetimes scale roughly as  $t_* \propto 1/M_*$ . For the upper branch of the main sequence, the longest-lived stars are those with the minimum mass required to burn  ${}^3\text{He}$  into  ${}^4\text{He}$ , where this mass scale is  $M_* \approx 0.03M_\odot$  (see Figures 4 and 5). These stars live for trillions of years, much longer than the expected lifetime of the Sun, and much longer than the current age of our universe. The stars on the lower degenerate branch of the main sequence, with  $M_* \lesssim 10M_J$ , can live even longer, up to  $\sim 10^{14}$  yr. However, these stars are dim and cool, with  $L_* \sim 10^{-7} - 10^{-8}L_\odot$  and  $T_* \sim 300$  K.

The central temperature is plotted as a function of stellar age in Figures 6 and 7 for the same collection of stars (with nuclear enhancement factors  $X = 10^{15}$  and  $X = 10^{18}$ ). Results are shown for stellar masses ranging from  $M_* = 0.5M_J$  up to  $M_* = 100M_\odot$ . All of the stars display an extended phase of nearly constant central temperature corresponding to burning of hydrogen into diprotons and then  ${}^3\text{He}$ . For higher mass stars, this temperature is somewhat higher than  $10^6$  K, whereas for lower mass stars, the central temperature is somewhat smaller than  $10^6$  K (for stellar mass  $M_* \gtrsim 10M_J$ ). For stars on the lower portion of the main sequence, with  $M_* < 10M_J$ , the central temperature is substantially lower. All of these central temperatures are below that required to process  ${}^3\text{He}$  into  ${}^4\text{He}$  (which corresponds to  $T_c \sim 7 \times 10^6$  K), so the stellar cores are converted into the lighter helium isotope. The time span for this  $p$ - $p$ -burning phase ranges from about 1 Myr for the largest stars ( $M_* \sim 100 M_\odot$ ), to 1 Gyr for solar type stars ( $M_* \sim 1M_\odot$ ), to 100 Gyr for the smallest stars on the upper main sequence ( $M_* \sim 0.01M_\odot$ ). As discussed above, stars on the lower degenerate branch of the main sequence can live up to  $10^{14}$  yr.

After the stellar cores exhaust their protons and attain a largely  ${}^3\text{He}$  composition, the stars condense, the central temperatures increases to  $\sim 10^7$  K, and  ${}^3\text{He}$  is processed into  ${}^4\text{He}$ . For the higher mass stars, this phase has a comparable lifetime to the earlier hydrogen burning phase (note the logarithmic scale). For lower mass stars, this second phase lasts even longer than the initial phase, as long as the stars are massive enough to burn  ${}^3\text{He}$ . The smallest stars, those with masses  $M_* \lesssim 0.025 M_\odot$  have enough mass to produce  ${}^3\text{He}$ , but not to burn it. As a result, the longest-lived stars (on the upper main sequence) are those with the minimum mass required to burn  ${}^3\text{He}$ , with  $M_* \approx 0.025M_\odot$ , where the total lifetime is  $\sim 5.5$  trillion years. For comparison, the longest-lived stars in our universe, with mass  $M_* = 0.08M_\odot$ , have main-sequence lifetimes of  $\sim 12$  trillion years [42]. Note that these timescales are calculated for stars with solar metallicity,  $\mathcal{Z} = \mathcal{Z}_\odot$ , and that lifetimes increase with increasing metallicity (up to a maximum value

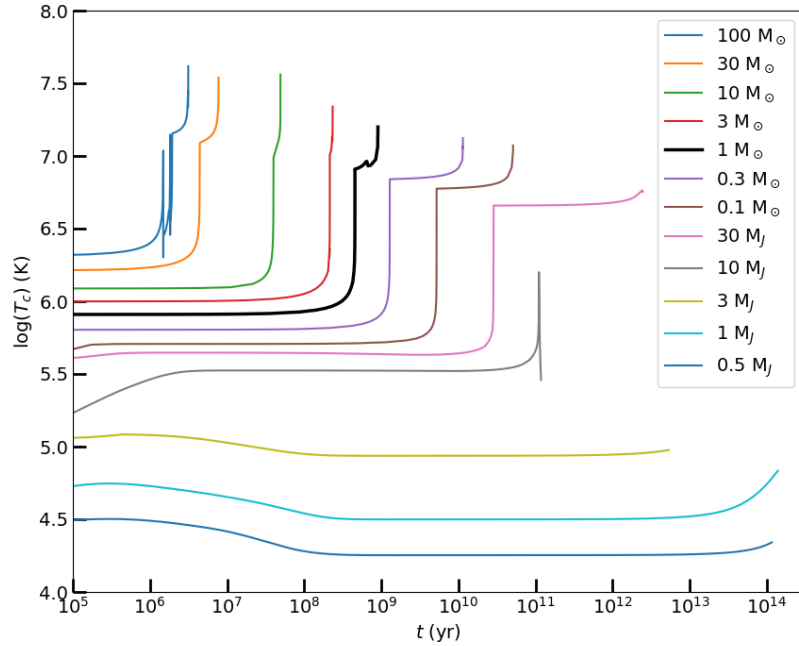


Figure 6: Central temperature as a function of stellar age for stars with nuclear enhancement factor  $X = 10^{15}$ .

$\mathcal{Z} \approx 0.04 > \mathcal{Z}_{\odot}$  [43]).

Figures 8 and 9 shows the tracks in the H-R diagram for stars with bound diprotons over the same age range used in the previous figures ( $X = 10^{15}$  and  $X = 10^{18}$ , respectively). The tracks start at stellar age  $t = 10^4$  yr, which is somewhat shorter than their expected formation time, in order to see how the stars evolve at early times. In this application, we use the *MESA* stellar evolution code to build stellar models with large radii and then follow their subsequent evolution onto the main-sequence. Future work should account for the star formation process, where the bodies actively assemble their masses over time spans of  $t_f \sim 10^5$  yr [44]. Although the initial decade in time should not be considered as definitive, for stellar ages  $t \gtrsim 10^5$  yr, the stellar tracks reflect the physical behavior that is expected. In Figures 8 and 9, the pre-main-sequence (PMS) portions of the tracks in the H-R diagram are confined to the right of the main sequence (lower surface temperatures) and are relatively short (and would be shorter if they were plotted after the isochrone for  $10^5$  yr).

The PMS phase for diproton stars is thus shorter than that of ordinary hydrogen burning stars, and this trend can be understood as follows: The central temperature is an increasing function of time as the stars contract. The central temperature ( $T_c \sim 10^6$  K) required for diproton reactions is reached well before

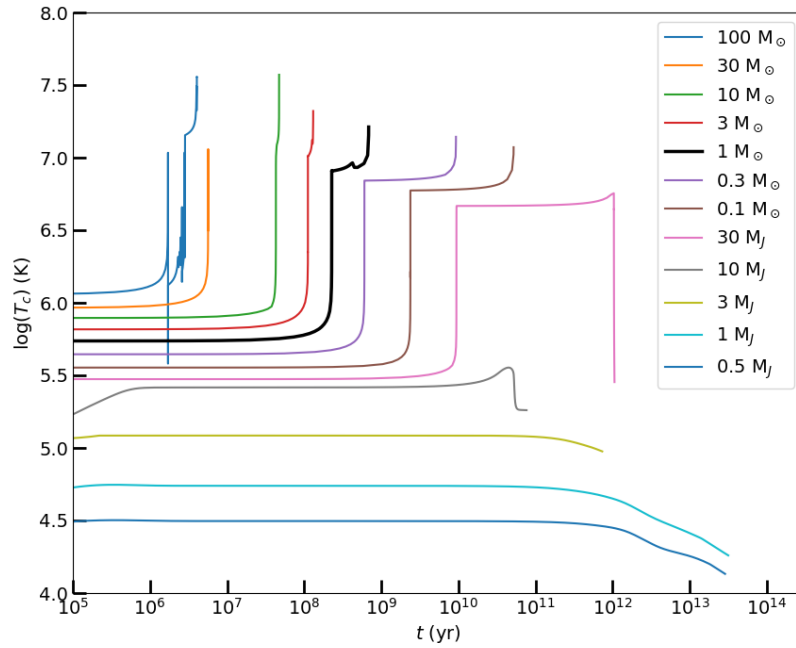


Figure 7: Central temperature as a function of stellar age for stars with nuclear enhancement factor  $X = 10^{18}$ .

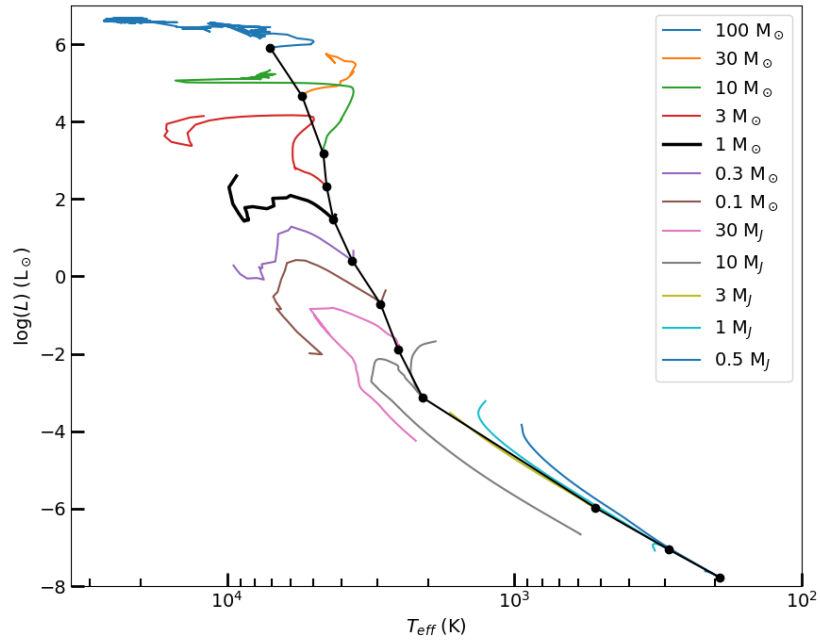


Figure 8: Tracks in the H-R diagram for stars with stable diprotons and nuclear enhancement factor  $X = 10^{15}$ . The black curve depicts the Zero Age Main Sequence, ZAMS, defined here as the epoch when the nuclear burning luminosity reaches 99% of the total luminosity. The tracks to the right of the main sequence corresponds to the early pre-main-sequence evolution, whereas the tracks to the left correspond to later post-main-sequence evolution.

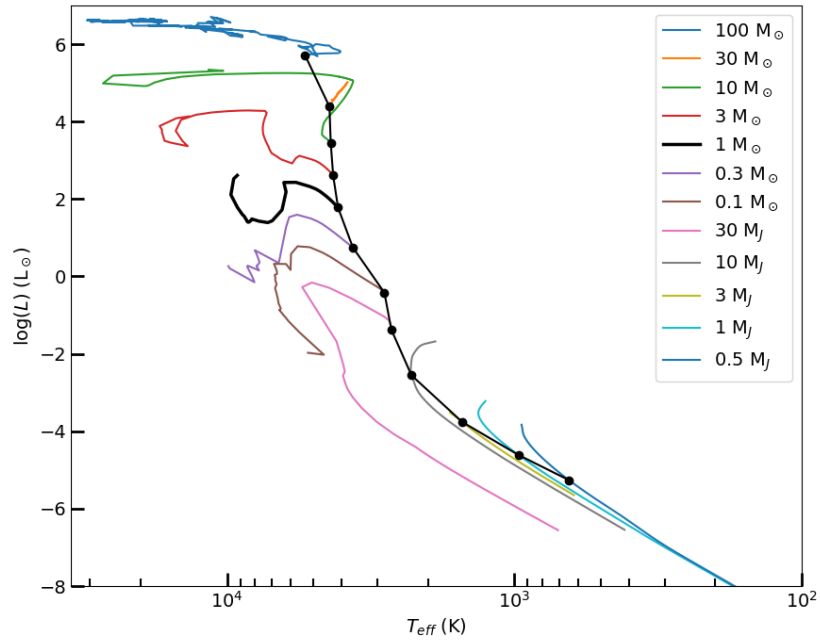


Figure 9: Tracks in the H-R diagram for stars with stable diprotons and nuclear enhancement factor  $X = 10^{18}$ . The black curve depicts the Zero Age Main Sequence, ZAMS, defined here as the epoch when the nuclear burning luminosity reaches 99% of the total luminosity. The tracks to the right of the main sequence corresponds to the early pre-main-sequence evolution, whereas the tracks to the left correspond to later post-main-sequence evolution.

the temperature ( $T_c \sim 1.5 \times 10^7$  K) required for hydrogen burning, resulting in the shorter PMS phase. When the central temperature reaches  $T_c \sim 10^6$  K, and nuclear fusion begins, the vertical evolution in the H-R diagram comes to a halt, and the stars lie along the zero-age main-sequence (shown as the dark curves in Figures 8 and 9).

Figures 8 and 9 also show the post main sequence evolution of the stars, up to the development of a helium core. These tracks indicate that stars move to the left in the H-R diagram (with increasing surface temperatures) as they exhaust their hydrogen and  ${}^3\text{He}$  fuel. Subsequent stellar evolution, where stars with  $M_* \gtrsim 1M_\odot$  produce carbon and successively larger nuclei, is expected to be the nearly same as in our universe for a given stellar mass, and the corresponding tracks are not shown. For the largest stars with  $M_* = 100M_\odot$ , the tracks display detailed structure, where the stars move back and forth in the diagram during their post main sequence evolution (upper dark blue curves). This complicated behavior arises because such large stars have enough internal radiation pressure that they approach  $n = 3$  polytropes, which are unstable [33, 34, 35]. Notice also that the tracks for low-mass stars, with masses  $M_* \lesssim 0.3M_\odot$ , turn downward (with decreasing luminosity) at the end of time span shown in the diagram. This behavior is expected: unlike solar-type (and more massive) stars, low-mass stars do not become red giants during their post main sequence evolution, and become bluer and dimmer instead [42].

#### 4.3. Mass-Luminosity Relation

In contrast to the standard mass-luminosity relation for radiative hydrogen burning stars on the main sequence, where  $L_* \propto M_*^3$ , these numerical results show that diproton stars have  $L_* \propto M_*^2$ . This trend holds over the entire upper branch of the main sequence, for stellar masses in the range  $M_* = 0.01 - 100 M_\odot$ . The key features leading to this form of the mass-luminosity relation are that both the central temperature and the surface temperature are almost constant — nearly independent of stellar mass — as discussed below.

First, consider the central temperature  $T_c$ . The enhanced cross sections for nuclear interactions lead to lower operating temperatures ( $T_c \sim 10^6$  K). As a result, the classical turning point for nuclear interactions is larger than for standard stellar interiors. Because the particles interact through quantum mechanical tunneling, which is exponentially suppressed, the reaction rate is extremely sensitive to temperature. The lower temperature implies a larger tunneling barrier, which makes the reaction rates an even more steeply increasing function of  $T_c$  (compared to main sequence stars in our universe). This extreme sensitivity, in turn, leads to a nearly constant central temperature as a function of stellar mass.

The surface temperature  $T_{\text{eff}}$  is also nearly constant with varying stellar mass, as shown by the main-sequence for diproton stars in the H-R diagram (Figure 2). This behavior is related to the Hayashi forbidden zone [41], which prevents stars from having surface temperatures that are too cool, and is caused primarily by opacity effects. Although the derivation is somewhat complicated, it can be shown that fully convective stars trace through nearly vertical tracks in the H-R diagram [34, 36], so that the surface temperature is nearly independent of luminosity and slowly varying with stellar mass. A simplified version of this argument is presented in Appendix B. These stars, which have larger luminosities from the production of diprotons, are largely convective and display this behavior.

Given central temperatures  $T_c$  and photospheric temperatures  $T_{\text{eff}}$  that are nearly constant, the mass-luminosity relation can be understood as follows. The central pressure of the star must be large enough to support the star against self-gravity and must be provided by the ideal gas law. These two constraints can be written in the approximate form

$$P_c \approx \frac{GM_*^2}{R_*^4} \approx \rho_c \frac{kT_c}{\mu} \approx \frac{M_* kT_c}{R_*^3 \mu}, \quad \text{or} \quad kT_c \approx \frac{GM_* \mu}{R_*}, \quad (43)$$

where we ignore dimensionless factors of order unity and where  $\mu$  is the mean particle mass in the stellar core. In the limit where  $T_c$  is independent of stellar mass, the above relations show that  $R_* \propto M_*$ . Now consider the outer boundary condition,

$$L_* = 4\pi R_*^2 \sigma T_{\text{eff}}^4. \quad (44)$$

For constant surface temperature, we find that

$$L_* \propto R_*^2 \propto M_*^2, \quad (45)$$

as found in the stellar evolution simulations. Putting in the physical constants, we can derive an approximate expression for the stellar luminosity as a function of mass:

$$L_* = 4\pi \left( \frac{GM_* \mu}{kT_c} \right)^2 \sigma T_{\text{eff}}^4. \quad (46)$$

This relation leads to the simple power-law  $L_* \sim M_*^2$  for constant  $T_c$  and  $T_{\text{eff}}$ .

For completeness we note that the expression (46) continues to be (approximately) valid even when the central temperature  $T_c$  and photospheric temperature  $T_{\text{eff}}$  vary with mass. In actuality, both the  $T_c$  and  $T_{\text{eff}}$  are slowly increasing functions of stellar mass. Moreover, the central temperature  $T_c$  varies more rapidly than the surface temperature  $T_{\text{eff}}$ . Figure 6 shows that  $T_c$  varies by a factor  $\sim 6.6$  over the allowed mass range, so that  $T_c^2$  varies by  $\sim 44$ . For comparison, Figure 2 shows that  $T_{\text{eff}}$  varies by a factor of  $\sim 2.5$ , so that  $T_{\text{eff}}^4$  varies by  $\sim 40$ . As a result,

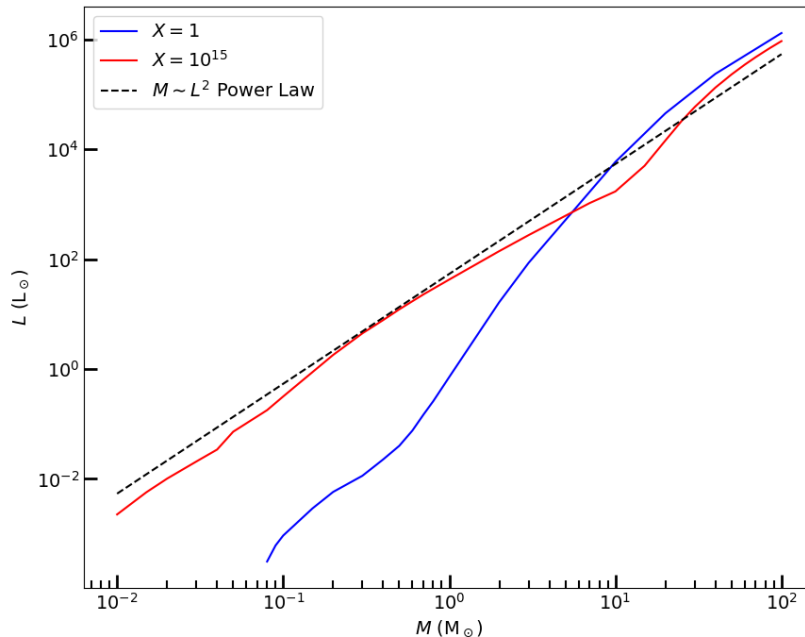


Figure 10: Mass-luminosity relationship for stars in universes with stable diprotons (with enhancement factor  $X = 10^{15}$ ). The red curve shows the mass-luminosity relation for the first stage of nuclear burning, where protons are processed first into diprotons and then into  ${}^3\text{He}$ . The dashed line shows the power-law relation from equation (46). For comparison, the blue curve shows the mass-luminosity relation for main sequence stars in our universe. Both sets of stellar models use solar metallicity.

the increase in  $T_c^2$  in the denominator is effectively offset by the increase in  $T_{\text{eff}}^4$  in the numerator, thereby leaving the original approximation  $L_* \sim M_*^2$  unchanged.

Figure 10 shows the mass-luminosity relationship for stars with stable diprotons on the upper branch of the main sequence ( $M_* = 0.01 - 100 M_\odot$ ), where the numerical results are compared to the analytic expression from equation (46). The red curve shows the relation calculated using the *MESA* code. The dashed line corresponds to the  $L_* \propto M_*^2$  relation resulting from constant central temperature  $T_c = 10^6$  K and constant photospheric temperature  $T_{\text{eff}} = 3000$  K. The power-law approximation works reasonably well over the four decades in stellar mass and (nearly) nine decades in stellar luminosity shown in the figure. For comparison, the blue curve shows the much steeper mass-luminosity relationship applicable for stars in our universe (note the smaller range in mass).

#### 4.4. Varying the Nuclear Enhancement Factor

In order to gain a clearer picture of the effects of the enhancement factor  $X$  on stellar evolution, this section considers a brief exploration of the possible parameter

space. Specifically, we simulate stars with mass  $M_* = 0.3 M_\odot$  for a wide range of the nuclear enhancement factors,  $X$ . Stars with this mass are sufficiently long-lived to support complex life over a large range in  $X$ , while still being massive enough to avoid the convergence issues associated with lower masses in *MESA*. Here we consider stars with values of the enhancement factor  $X$  from  $10^{-3}$  to  $10^{18}$ . For  $X < 10^{-3}$ , stellar evolution is dominated by the CNO cycle even for low-mass stars with  $M_* = 0.3 M_\odot$ , so that further reduction of the enhancement factor has negligible effect. For larger enhancements,  $X > 10^{18}$ , significant nuclear burning takes place during the pre-main-sequence phase, so that the star formation process (accretion history) must be included in the *MESA* simulations.<sup>4</sup>

The evolution of  $M_* = 0.3M_\odot$  stars in the H-R diagram is depicted in Figure 11 over a range of 21 orders of magnitude in the nuclear enhancement factor  $X$ . Since the stellar mass is held constant, each star descends the same pre-main-sequence (Hayashi) track until it reaches the central temperature necessary to initiate fusion for a given level of enhancement. The star then reaches the main sequence. For clarity, we also plot the effective temperature  $T_*$  as a function of time for these objects in Figure 12. The photospheric temperature remains nearly constant, with  $T_* \sim 3500$  K, over the full range of enhancement factors, although the lifetime decreases with increasing  $X$ . For stars with  $X \leq 1$ , the hydrogen burning temperature is high enough that  ${}^3\text{He}$  is burned into  ${}^4\text{He}$  at the same time. For larger values of  $X \geq 10^3$ , however, this latter reaction takes place later in a separate phase of evolution, and the surface temperatures increase to  $T_* \sim 7000 - 8000$  K. Taken together, Figures 11 and 12 indicate that this blueward excursion in the H-R diagram is associated with the transition from  $p$ - $p$  fusion to  ${}^3\text{He}$  fusion. Keep in mind that the initial  $p$ - $p$  -burning stage remains near the Hayashi track, as we saw with the  $X = 10^{15} - 10^{18}$  cases above.

To further elucidate the evolution of these objects, Figure 13 shows the luminosity as a function of time, and Figure 14 shows the central temperature versus time. These plots cleanly demonstrate the (nearly) logarithmic dependence of luminosity, central temperature, and stellar lifetime on the enhancement factor. This dependence is specific to the  $p$ - $p$  burning stage, which corresponds to the extended phase of evolution with constant luminosity and central temperature (for a given

---

<sup>4</sup>As mentioned above, in this application, we do not simulate the formation of stars, but rather use *MESA* to construct pre-main-sequence models with arbitrarily large radii and then let them evolve toward a hydrogen burning state. As a result, the earliest stages of evolution do not necessarily reflect the true history of the star. Nonetheless, the models rapidly converge (in time) towards physically realistic states.

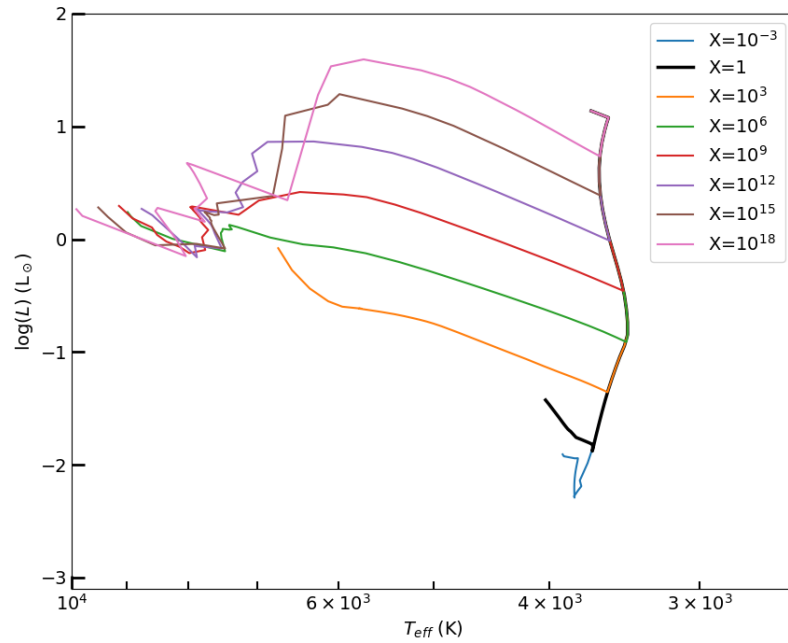


Figure 11: Tracks in the H-R diagram for stars with  $M_* = 0.3 M_\odot$  and varying values of the nuclear enhancement factor. The enhancement factor varies over the range  $X = 10^{-3} - 10^{18}$ , as labeled. All of the stellar models show the same initial evolution as they contract and move nearly vertically down the Hayashi track. Contraction halts when the central temperature  $T_c$  reaches that required for nuclear burning, where the  $T_c$  decreases (slowly) with increasing degrees of nuclear enhancement.

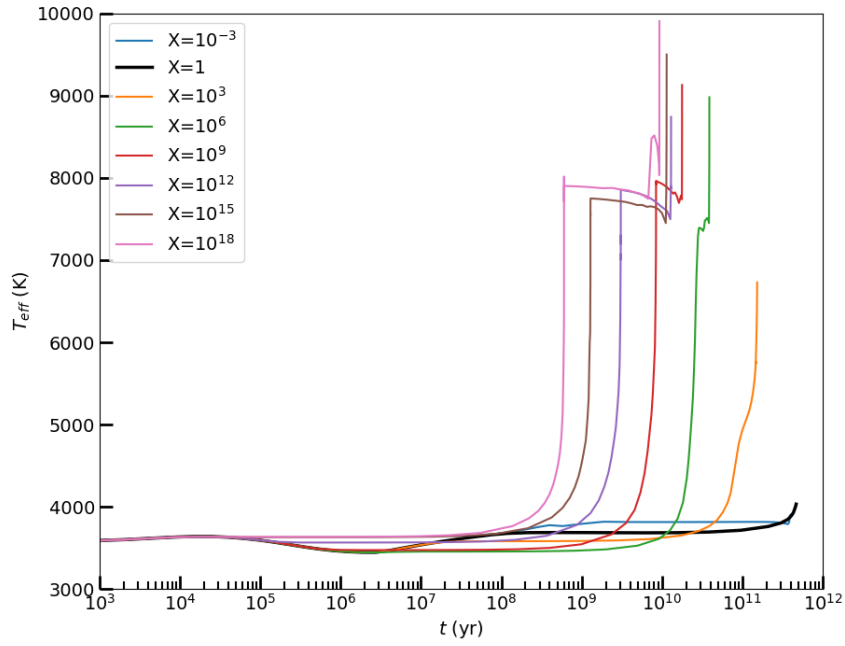


Figure 12: Photospheric temperature  $T_*$  as a function of time for stars with  $M_* = 0.3M_\odot$  and varying values of the nuclear enhancement factor  $X$  (as labeled). All of the stars have surface temperatures  $T_* \sim 3500$  K during both their pre-main-sequence phase and on their initial main sequence tracks, burning protons to diprotons and then  ${}^3\text{He}$ . For stars with  $X \geq 10^3$ , the  ${}^3\text{He}$  is not processed promptly into  ${}^4\text{He}$ , which is then produced later in separate phase with larger photospheric temperature. For stars in our universe (and for  $X < 1$ ),  ${}^4\text{He}$  is produced promptly and the surface temperature remains low (black and blue curves).

$X$ ). In contrast, the later  ${}^3\text{He}$ -burning stage takes place through strong reactions, and is therefore not significantly affected by the enhancement factor. This logarithmic dependence further illustrates the robust nature of stellar evolution in the face of changes in nuclear physics.

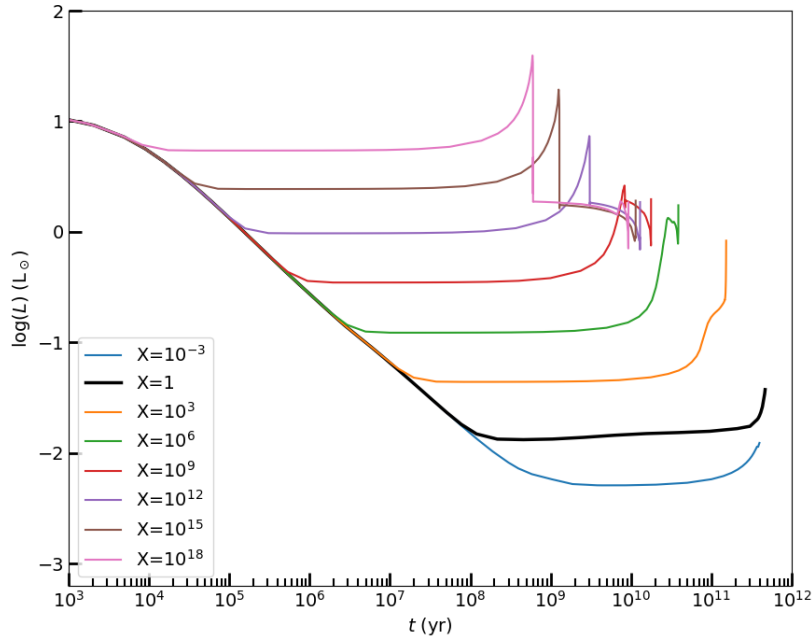


Figure 13: Stellar luminosity  $L_*$  as a function of time for stars with  $M_* = 0.3M_\odot$  and varying values of the nuclear enhancement factor (as labeled). The luminosity decreases with time as the stars contract toward the main sequence, and then reaches a constant value when nuclear burning begins. The luminosity level increases slowly with increasing nuclear enhancement factor,  $X$ .

#### 4.5. Degenerate Very Low-Mass Stars

One surprising result from our simulations is that nuclear burning still occurs in very low-mass stars with masses  $M_* \sim 1 - 10M_J$ , below the deuterium-burning limit. These objects look significantly different from other low-mass stars. With radii comparable to that of Jupiter, these objects begin their evolution on cooling tracks similar to brown dwarfs and eventually attain surface temperatures far

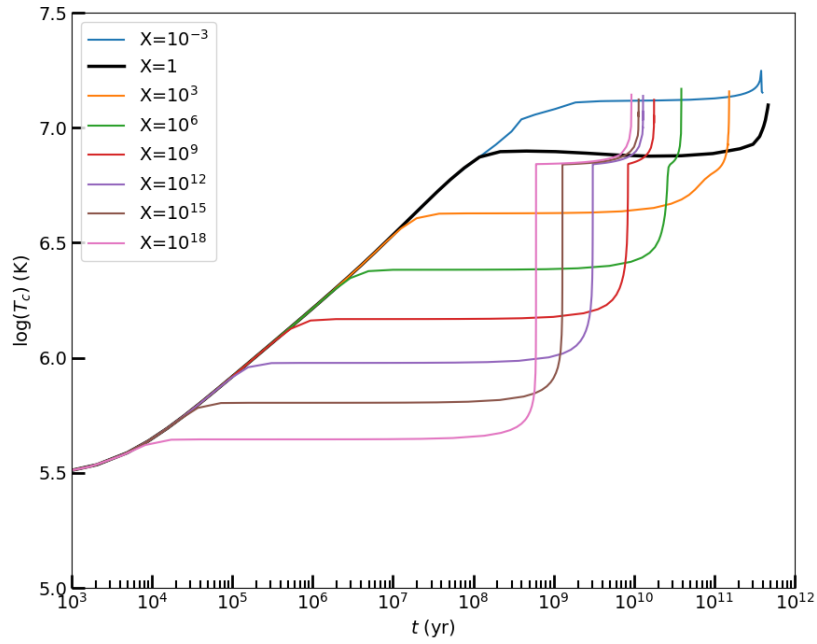


Figure 14: Central temperature  $T_c$  as a function of time for stars with  $M_* = 0.3M_\odot$  and varying values of the nuclear enhancement factor (as labeled). The central temperature increases with time until nuclear burning begins, where the ignition temperature decreases with increasing values of the nuclear enhancement factor,  $X$ . For stars in our universe (black curve), the nuclear burning temperature is high enough that  ${}^3\text{He}$  is burned into  ${}^4\text{He}$  during the (single) main sequence phase. For enhanced reaction rates, roughly  $X > 10^3$ , the central temperature of the first phase is below that needed to burn  ${}^3\text{He}$ , which is processed during a later phase when  $T_c$  abruptly increases to  $\sim 10^7$  K.

below the Hayashi limit for non-degenerate objects. The smallest of these objects have surface temperatures  $T_* < 300$  K, making them “frozen stars” where ice crystals could form in their atmospheres. Moreover, the central temperatures of these objects are  $T_c = 3 \times 10^4 - 10^5$  K, which is normally considered too low to sustain nuclear burning, even with strong (or electromagnetic) reactions.

It is possible that such unusual results are due to shortcomings in the equation of state (or opacities) under the extreme conditions realized in these objects. Nonetheless, a close inspection of the simulations reveals that these objects are indeed physically plausible. An order of magnitude treatment of the conditions required for nuclear burning is carried out in Appendix C. These objects are partially degenerate, so that their hydrostatic equilibrium is largely independent of nuclear reactions. In the extreme limit, degeneracy can support the star against gravity, while nuclear reactions take place in the background — at an attenuated rate — provided that the nuclear enhancement factor (and hence the reaction cross section) is large enough. The enormous densities associated with degenerate objects lead to strong electron screening, which negates some of the Coulomb repulsion and allows for nuclear reactions to occur at lower central temperatures. Nuclear burning is often described as “switching on” at some specified temperature. Yet, although the reaction rates are exponentially dependent on temperature, they are always taking place at some low level. Non-degenerate objects cannot be supported in such a regime, and must adjust to another stellar configuration. However, the very low-mass objects considered here are largely supported without their nuclear contribution, so that these objects can generate energy at anemic rates. With their low central temperature, the associated nuclear burning rate is extremely slow, such that the stellar lifetime is longer than  $10^{14}$  years, despite the lower yield of burning to  ${}^3\text{He}$  rather than  ${}^4\text{He}$ . With low luminosity and fixed radius, these objects can thus maintain surface temperatures  $T_* \sim 300$  K.

The strange properties of these hypothetical very low-mass stars stem from them being partially degenerate, like brown dwarfs. Under these conditions, the central region of the star (where nuclear burning occurs) does not need to reach a pressure equilibrium to support the star against gravity, but is still able to reach and maintain a *thermal* equilibrium. This latter condition is reached at a much lower temperature (compared with that required for pressure equilibrium). After  $\sim 10^9$  yr, the nuclear burning luminosity dominates over heating from Kelvin-Helmholtz contraction, and the “star” can function as a nuclear-burning entity.

Note that the possibility of this unusual stellar state is a result of strong-burning nuclear reactions in general rather than the  $p(p, {}^2p)\gamma$  reaction in particular. Intriguingly, this finding suggests that if Jupiter were made of pure deuterium in our own universe, it could also reach a thermal equilibrium of nuclear burning. It also suggests that similar very low-mass stars could occur in a “weakless” universe

[25]. In previous work [26], we found that in some universes without a weak interaction, stars will be composed mostly of deuterium and will produce energy via strong reactions, but we did not explore stars smaller than the standard deuterium burning limit. Nonetheless, very low-mass degenerate stars in such a universe could operate by the same mechanism.

The minimum mass of these degenerate stars depends on the enhancement factor, but appears to be significantly less than  $\sim 1M_J$ . We were not able to definitively determine this minimum mass from our simulations because of convergence problems at low masses (primarily due to the equation of state for the extreme conditions associated with these very low-mass stars). The smallest star that we were able to successfully simulate had mass  $M_* = 0.5 M_J$ . However, simulations run with a range of enhancement factors suggest that the minimum stellar mass lies in the neighborhood of  $M_* = 0.25 M_J$  for  $X = 10^{15}$ . For lower masses, the nuclear burning luminosity never exceeds the Kelvin-Helmholtz luminosity, and the object evolves as an ordinary sub-brown dwarf or giant planet.

## 5. Conclusion

This paper has considered stellar evolution in universes with stable diprotons. In this scenario, nuclear reactions can take place in stellar cores through the strong force, with reaction rates enhanced by factors  $X \sim 10^{15} - 10^{18}$ . Our main results are summarized in Section 5.1, with a discussion of their implications presented in Section 5.2.

### 5.1. Summary of Results

The most important result of this study is that stars continue to operate normally with large enhancements of their nuclear reaction cross sections, such as those expected in universes with stable diprotons. The stellar luminosities, lifetimes, and surface temperatures are roughly similar to those of stars in our universe. Although some differences arise, as described below, these stars do not have catastrophically short lifetimes (as many previous papers have asserted, e.g., [7, 8, 9, 10, 11, 12, 13, 14, 15]). The longest-lived stars can sustain nuclear fusion for trillions of years, about three orders of magnitude longer than the current age of our universe.

Considerations of Big Bang Nucleosynthesis with bound diprotons (Section 2) indicate that the abundances of protons, deuterium, and helium will be approximately the same as in standard BBN. The production of diprotons is suppressed relative to deuterium because of the coulomb barrier, in spite of the enhanced cross section. The diprotons that are produced will eventually be transmuted into deuterium, thereby raising its abundance. Nonetheless, we expect  $Y_d \ll Y_p$ , so

that the starting conditions for stellar evolution and nucleosynthesis are largely unchanged (see also [21, 22]).

The main sequence for stars with stable diprotons can be separated into two branches (Figure 2). The upper main sequence corresponds to stellar masses  $M_* = 0.01 - 100M_\odot$ . Compared to stars with standard nuclear reaction rates, these stars are somewhat more luminous and have redder surfaces. As a result, the main sequence for these objects is steeper than the standard one, with surface temperatures spanning the narrower range  $T_{\text{eff}} \sim 2500 - 5500$  (see Figure 2). The largest stars (with  $M_* = 100M_\odot$ ) have approximately the same luminosity as those in our universe, whereas lower mass stars have higher luminosity. As a result, the luminosity range is compressed for the same span of stellar masses. However, this trend is compensated for by the larger range in stellar mass that can sustain nuclear burning. Over the upper main sequence, with masses  $M_* = 0.01 - 100M_\odot$ , the overall range in stellar luminosity is roughly comparable to that of our universe, i.e.,  $L_* \sim 10^{-3} - 10^6 L_\odot$ . The solar-type stars, with somewhat cooler surfaces and more luminosity than our Sun, have configurations roughly similar to those of red giants in our universe. Note that this same set of stellar properties arises for stars that are primarily composed of deuterium [26, 27], which has nuclear reaction rates comparable to those of diprotons.

In addition to stars that are supported by the pressure resulting from their internal nuclear reactions, the greatly enhanced reaction rates allow for a new type of hybrid stellar configuration that corresponds to the lower “degenerate branch” of the main sequence shown in Figure 2. Stellar objects with masses  $M_* = 1 - 10M_J$  can be supported (in part) by degeneracy pressure, but still sustain nuclear reaction rates high enough to produce quasi-stable surface temperatures  $T_* \sim 300$  K. These objects are like brown dwarfs in our universe in that they do not generate enough power to be supported through thermal pressure. On the other hand, the residual nuclear reactions are effective enough that the bodies can maintain a nearly constant luminosity over extended time scales (see Section 4.5 and Appendix C).

For masses comparable to the Sun, the lifetimes for stars with stable diprotons are shorter than those burning hydrogen by about one order of magnitude (see Figures 4 – 7). low-mass stars live much longer than larger stars, so that stars with  $M_* \approx 0.3M_\odot$  have main-sequence lifetimes comparable to solar-type stars with standard nuclear reactions. Moreover, because of the much larger cross sections for diproton reactions, stars in such universes can sustain nuclear reactions with much smaller masses than in our universe, so that the upper main sequence extends down to masses  $M_* \approx 0.01M_\odot$ , with commensurately longer lifetimes. These results vary logarithmically with the enhancement factor  $X$  (see Section 4.4 and Appendix D).

The range of stellar masses for the upper main sequence thus spans a factor of  $\sim 10^4$ , with an additional decade in mass contributed by the lower main sequence,

compared with a mass range of  $\sim 10^3$  in our universe. With a larger range in mass, and a similar range in luminosity, the mass-luminosity relation over the upper main sequence is less steep than that of our universe. To a good approximation, we find  $L_* \propto M_*^2$  (see Figure 10), and this result can be understood in terms of basic stellar physics (see Section 4.3 and Appendix B).

With greatly enhanced reaction cross sections, the usual  $p$ - $p$  chain of nuclear reactions takes place in two stages. In the first stage, protons fuse into diprotons, which capture electrons to become deuterium and then interact with protons to become  $^3\text{He}$ . Because of the lower nuclear burning temperature for this process, the fusion of  $^3\text{He}$  into alpha particles does not take place promptly, but rather occurs later during the second stage. The smallest stars can sustain nuclear fusion and produce  $^3\text{He}$ , but do not have enough mass to process the  $^3\text{He}$  into  $^4\text{He}$  (which requires a higher central temperature). As a result, the longest-lived (non-degenerate) stars in universes with stable diprotons have masses  $M_* \approx 0.025M_\odot$ , the minimum needed to produce  $^4\text{He}$ , and live for  $t \sim 6000$  Gyr. This lifetime is comparable to that of the longest-lived stars in our universe ( $M_* = 0.08M_\odot$  and  $t \sim 10^4$  Gyr) and much longer than the current cosmic age ( $\sim 14$  Gyr). The partially degenerate stars on the lower main sequence can sustain nuclear processes even longer, up to  $t \sim 10^5$  Gyr.

## 5.2. Discussion

The main result of this paper is that stellar evolution is only modestly affected by the greatly enhanced nuclear reaction cross sections expected in universes with stable diprotons. In particular, the smallest such stars can still live for trillions of years, far beyond the current age of the universe. Since this finding is in stark contrast to many previous claims in the literature, it is useful to elucidate why stars are so impervious to changes in the input nuclear physics.

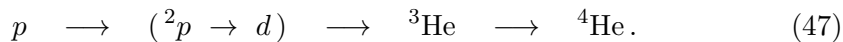
First, note that stellar lifetimes do not vary inversely with the nuclear reaction cross sections, but only logarithmically. The energy generation rate in the stellar core must compensate for the energy lost from the stellar surface, but stars can adjust their reaction rates by expanding or contracting. Since pressure is provided by the ideal gas law, changes in stellar radius lead to corresponding changes in the core temperature. The nuclear reaction rates are exponentially sensitive to temperature, so that a small decrease in  $T_c$  can compensate for an enormous increase in the cross section. Specifically, for enhancement factors in the range  $X = 10^{15} - 10^{18}$ , the operating temperature of stars decreases from  $T_c \approx 1.5 \times 10^7$  K (the value for our Sun) down to about  $T_c \sim 10^6$  K. This modest change in  $T_c$  lowers the nuclear reaction rate by a factor comparable to the enhancement factor  $X$  of the cross section. The reason for the extreme sensitivity is that the nuclear reactions take place via quantum mechanical tunneling, and the barriers

are substantial. In the core of the Sun, for example, the typical proton separation (24,000 fm) and the classical turning point ( $\sim 1000$  fm) are both much larger than the range of the strong force ( $\sim 10$  fm). The protons thus have a formidable barrier to tunnel through.

The characteristic temperature of  $T_c \sim 10^6$  K for stars with stable diprotons is essentially equivalent to the well-known deuterium burning temperature [45]. This coincidence is not surprising, because the reaction cross section for deuterium burning is larger than that for the standard  $p$ - $p$  chain by a factor of  $\sim 10^{18}$ , and deuterium reactions are the strong-force analog reactions used to estimate the enhancement factors for diproton reactions.

In our universe, most stars experience a deuterium burning phase during their early evolution. Stars are born with radii too large and central temperatures too low to sustain hydrogen fusion.<sup>5</sup> As a result, newly born stars are not powered by nuclear reactions, but rather by gravitational contraction. During this pre-main-sequence phase, the stellar radius decreases and the central temperature grows. When the temperature becomes high enough,  $T_c \sim 10^6$  K, deuterium burning commences and delays further contraction. Because the deuterium abundance is low,  $D/H \sim 2 \times 10^{-5}$ , this phase only lasts for  $\sim 10^5$  years before the deuterium fuel is exhausted in the stellar core. Some time later, 0.1 – 10 Myr depending on the stellar mass, the core reaches the higher temperature ( $T_c \sim 1.5 \times 10^7$  K) necessary for hydrogen burning. In universes with bound diprotons and enhanced nuclear cross sections, however, stars can burn through the bulk of their fuel with central temperatures  $T_c \sim 10^6$  K. Since the nuclear fuel is more abundant by a factor  $\sim 10^5$  (compared to the deuterium supply in our universe), solar type stars can sustain nuclear fusion for billions of years.

In this consideration of universes with bound diprotons, we are assuming that the strong force is somewhat stronger than in our universe (with an increase of order  $\sim 10\%$ , [8, 9, 12, 13]). However, apart from the existence of the bound state  ${}^2p$  and enormous enhancements of the cross sections ( $X = 10^{15} - 10^{18}$ ), we are implicitly assuming that the rest of nuclear physics is largely unchanged. In particular, the particle spins are the same as in our universe, and the ordering of nuclear binding energies remains constant. These properties imply that nucleons will cascade into larger nuclei as in our universe, with the progression



One expects the weak force to vary along with the strong force, but the modest

---

<sup>5</sup>This discussion applies only to stars with masses  $M_* \lesssim 7 M_\odot$ . The largest stars, corresponding to the most massive  $\sim 1\%$  of the stellar population, burn their deuterium as they form.

changes considered here will not affect stellar operations. If anything, the key process of electron capture from equation (20) will be even more effective.

Although the expected small changes in binding energy do not affect the progression from protons to helium outlined above, the later stages of nuclear burning in massive stars could be altered. In this regime, relatively small changes in binding energies could lead to interesting systematic differences [33, 34]. As nuclei of ever larger atomic number undergo nuclear burning, the time scales decrease (down to minutes and even seconds), and the reaction networks become increasingly complicated. As a result, the relative abundances of heavy elements (up to iron and beyond) produced by massive stars could be somewhat different in universes with stable diprotons. This issue is beyond the scope of this present paper and is left for future work.

One should keep in mind that much larger changes to the strong force can affect nuclear structure and the manner in which stars evolve. This issue is complicated by the nature of the strong interaction, which is ultimately determined through QCD, but can be described by an effective nuclear potential with an overall strength, a length scale (range), and a repulsive core (e.g., see [46] and references therein). Quantum statistics also plays an important role, especially for light nuclei, as bound states must be overall antisymmetric in spin and isospin. All of these components to the potential will affect nuclear structure. As an extreme example, if the strong force becomes much stronger, then nucleons become relativistic in their bound nuclear states. In addition, the nuclei could transform to states of quark matter, where free quarks provide the degrees of freedom instead of protons and neutrons. The required variations to the strong force potential necessary to instigate these changes has not been determined. Since nuclear binding energies are of order 1 MeV per particle, and the QCD phase transition temperature is  $\sim 200$  MeV (and nucleon masses are  $\sim 1$  GeV), an increase in the strong force by a factor of  $\sim 100$  could lead to vastly different nuclear structures. Even in this case, the nuclei could remain as bound entities, and their role in atomic physics would be essentially unchanged. However, the astrophysical processes that produce the nuclei, in BBN and stellar nucleosynthesis, could be quite different. (For example, as noted in Section 4.4, if these changes result in enhancement factors  $X \gtrsim 10^{18}$ , nuclear burning would be able to occur during star formation.) These issues should be explored in future work.

This study demonstrates that stars are much less sensitive to variations in the fundamental parameters of physics and astrophysics than is often claimed. This work shows that stars operate normally even with enormous enhancements (15 – 18 orders of magnitude) in their nuclear reaction cross sections, as expected in universes with stable diprotons (see also [6, 20]). Previous work has shown that stars can maintain stable nuclear burning configurations with the fine structure

constant a factor of  $\sim 100$  larger or smaller, and with an even larger possible range for the gravitational constant [18, 19]. Stars can also function in universes with no weak interactions [26], stronger weak interactions [27], stable beryllium-8 [47], over a large range of carbon-12 resonances [48, 49, 50, 51], and even in universes without stable deuterium [52] (cf. [53]). Taken together, these findings indicate that stars are not the limiting factor for universes to remain habitable.

**Acknowledgments:** We are grateful to Martin Rees and Frank Timmes for useful feedback. The work of FCA is supported in part by NASA Grant NNX16AB47G and by the Leinweber Center for Theoretical Physics at the University of Michigan. AH is supported by an appointment to the NASA Postdoctoral Program at the NASA Goddard Space Flight Center, administered by Universities Space Research Association under contract with NASA. EG and GF acknowledge additional support from the National Science Foundation, Grant PHY-1630782, and the Heising-Simons Foundation, Grant 2017-228. GF also acknowledges NSF grant PHY-1914242 at University of California San Diego.

## Appendix A. Additional Nuclear Reactions

The existence of bound states of two protons ( ${}^2p$ ) and/or two neutrons ( ${}^2n$ ) requires the inclusion of new nuclear reactions. The possible reactions for light elements are listed in Table A.2 and are organized into different categories. The cross sections — and hence the reaction rates — for these new processes are expected to be comparable to those of analog reactions that exist in our universe (also shown in the table). For the reactions that include diprotons, we can add a neutron to one of the reactants on both sides of the equation and obtain an analog reaction with a known/measured reaction rate. The diproton becomes  ${}^3\text{He}$  under this procedure. Similarly, for reactions that involve the dineutron, we can add a proton to both sides of the reaction to obtain an analog process. In this case, the dineutron becomes tritium. We assume here that the analog reactions, which have known cross sections, will provide order of magnitude estimates for the new reactions. Note that the cross sections depend on the spin, charge, and mass of the participating particles. As a result, the analog cross sections can be different from the values for the new reactions by factors of order unity. For completeness we note that for the analog reactions involving tritium ( $t$ ), the reacting particles have increased charges and hence different Gamow factors. At low energies, the analog tritium reactions will thus be suppressed relative to the diproton/dineutron reactions (although these reactions do not play an important role in the stellar evolution calculations of this paper).

## Nuclear Reactions for Diprotons and Dineutrons

Reaction Type	New Reaction	Analog Reaction
Production	$p(p, \gamma) {}^2p$ $n(n, \gamma) {}^2n$	$d(p, \gamma) {}^3\text{He}$ $d(n, \gamma) t$
Weak	${}^2p(e^-, \nu_e) d$ ${}^2n(e^+, \bar{\nu}_e) d$	${}^3\text{He}(e^-, \nu_e) t$ $t(e^+, \bar{\nu}_e) {}^3\text{He}$
Single Nucleon	${}^2p(n, p) d$ ${}^2p(n, \gamma) {}^3\text{He}$ ${}^2n(p, n) d$ ${}^2n(p, \gamma) t$	${}^3\text{He}(n, d) d$ ${}^3\text{He}(n, \gamma) {}^4\text{He}$ $t(p, n) {}^3\text{He}$ $t(p, \gamma) {}^4\text{He}$
Diproton + Dineutron	${}^2p({}^2n, \gamma) {}^4\text{He}$ ${}^2p({}^2n, n) {}^3\text{He}$ ${}^2p({}^2n, p) t$ ${}^2p({}^2n, d) d$	${}^3\text{He}(t, \gamma) {}^6\text{Li}$ ${}^3\text{He}(t, d) {}^4\text{He}$ ${}^3\text{He}(t, d) {}^4\text{He}$ ${}^3\text{He}(t, t) {}^3\text{He}$
Deuteron	${}^2p(d, p) {}^3\text{He}$ ${}^2n(d, n) t$	${}^3\text{He}(d, p) {}^4\text{He}$ $t(d, n) {}^4\text{He}$
$A = 3$ Targets	$t({}^2p, p) {}^4\text{He}$ $t({}^2p, d) {}^3\text{He}$ ${}^3\text{He}({}^2n, n) {}^4\text{He}$ ${}^3\text{He}({}^2n, d) t$	${}^3\text{He}(t, d) {}^4\text{He}$ ${}^3\text{He}(t, t) {}^3\text{He}$ ${}^3\text{He}(t, d) {}^4\text{He}$ ${}^3\text{He}(t, t) {}^3\text{He}$
Helium Targets	${}^4\text{He}({}^2p, \gamma) {}^6\text{Be}$ ${}^4\text{He}({}^2p, {}^3\text{He}) {}^3\text{He}$ ${}^4\text{He}({}^2n, \gamma) {}^6\text{He}$ ${}^4\text{He}({}^2n, t) t$	${}^4\text{He}({}^3\text{He}, \gamma) {}^7\text{Be}$ ${}^4\text{He}({}^3\text{He}, {}^3\text{He}) {}^4\text{He}$ ${}^4\text{He}(t, \gamma) {}^7\text{Li}$ ${}^4\text{He}(t, t) {}^4\text{He}$

Table A.2: Nuclear reactions involving diprotons and dineutrons. The reactions can be grouped according to the type of particles involved as specified in the first column. New reactions involving diprotons and dineutrons are listed in the second column. Analog nuclear reactions that operate in our universe, and which are expected to have comparable cross sections, are listed in third column.

## Appendix B. Photospheric Temperatures for Convective Stars

This Appendix shows that fully convective stars have nearly constant surface temperature as a function of stellar mass. For the stars of interest, the enhanced interaction cross sections lead to somewhat larger luminosities, and the convective approximation provides a good model. These stars can be described by  $n = 3/2$  polytropes, where the equation of state takes the form

$$P = K\rho^{5/3}. \quad (\text{B.1})$$

This equation of state can be rewritten in terms of temperature

$$P = C(kT)^{5/2}, \quad (\text{B.2})$$

where we have assumed that the ideal gas law holds. Since the star is a complete polytrope, the constant  $C$  has the same value throughout the stellar interior, and can be written in terms of the mass and radius [36], i.e.,

$$C = \alpha G^{-3/2} \mu^{-5/2} M_*^{-1/2} R_*^{-3/2}, \quad (\text{B.3})$$

where  $\mu$  is the mean molecular weight of the gas. The dimensionless constant  $\alpha$  is independent of the mass and radius ( $M_*$ ,  $R_*$ ).

The pressure at the photosphere can be written in the form

$$P_* = \frac{2 g_*}{3 \kappa_*} = \frac{2}{3 \kappa_*} \frac{GM_*}{R_*^2}, \quad (\text{B.4})$$

where  $\kappa_*$  is the photospheric opacity. This expression follows from assuming hydrostatic equilibrium and using the fact that the optical depth  $\tau = 2/3$  at the photosphere. We can combine the expressions (B.2) and (B.4) for the photospheric pressure, along with the definition (B.3), to find

$$P_* = \frac{2}{3 \kappa_*} \frac{GM_*}{R_*^2} = \alpha G^{-3/2} \mu^{-5/2} M_*^{-1/2} R_*^{-3/2} (kT_{\text{eff}})^{5/2}. \quad (\text{B.5})$$

After some rearrangement this expression becomes

$$(kT_{\text{eff}})^{5/2} \kappa_*(T_{\text{eff}}) = \frac{2}{3\alpha} G^{5/2} \mu^{5/2} M_*^{3/2} R_*^{-1/2}, \quad (\text{B.6})$$

which shows how the temperature dependent quantities scale with stellar mass, radius, and composition. Now consider the standard case where the opacity at the photosphere is extremely sensitive to the temperature. The opacity is generally

dominated by interaction with  $\text{H}^-$ , and this opacity has an approximate temperature dependence of  $\kappa_* \sim T^9$ . If we use this power-law form for the opacity, we obtain the scaling law

$$T_{\text{eff}} \propto \mu^{5/23} M_*^{3/23} R_*^{-1/23}. \quad (\text{B.7})$$

The weak dependence on the stellar parameters  $(M_*, R_*)$  thus shows that the photospheric temperature is slowly varying across the main sequence, as long as the star remains convective.

Starting from equation (B.7), we can derive two additional scaling relations. First, we can use the surface boundary condition of equation (44) to eliminate the dependence on the radius  $R_*$  in favor of the luminosity  $L_*$ . This substitution yields the expression

$$T_{\text{eff}} \propto \mu^{5/21} M_*^{3/21} L_*^{-1/42}. \quad (\text{B.8})$$

Alternatively, as a consistency check, we can use the fact that the mass-luminosity relation has the form  $L_* \sim M_*^2$ , which implies that  $R_* \sim M_*$ . Using this latter result in equation (B.7), we find

$$T_{\text{eff}} \propto \mu^{5/23} M_*^{2/23}. \quad (\text{B.9})$$

Note that the exponents in all of the above scaling laws are small, so that the photospheric temperature  $T_{\text{eff}}$  is nearly constant across the range of stellar masses. The surface temperature is not exactly constant, however, but instead slowly varies with stellar mass. The main sequence spans four orders of magnitude in mass, but the corresponding range in surface temperature according to equation (B.9) is only a factor  $f \approx 10^{8/23} \approx 2.2$ . This range in  $T_{\text{eff}}$  agrees with that seen in the H-R diagram (see Figure 2).

The above derivation is approximate. More complicated treatments [34, 36] include the fact that the stellar photosphere is actually a thin radiative layer that matches smoothly onto the convective interior just below the surface. Other approximations for the opacity are also used, but as long as the opacity is a sensitive function of temperature, the scaling exponents are small, so that  $T_{\text{eff}}$  varies slowly with stellar mass.

## Appendix C. Degenerate Nuclear Burning Stars

The numerical simulations show that for sufficiently large enhancement factors, stars with low masses in the approximate range  $M_* = 1 - 10 M_J$  can sustain nuclear fusion at highly attenuated rates. Unlike somewhat larger stars in the range  $M_* = 10 - 100 M_J$ , which are also operational, these very low-mass objects are partially degenerate, with pressure contributions from both the ideal gas law and

electrostatic forces, but nonetheless can generate power. This Appendix outlines the physics of these unusual stars.

To a first approximation, the stars have constant radius as a function of mass (for sufficiently small  $M_* \leq 10M_J$ ). Fully degenerate stars would have the mass-radius relation  $R_* \sim M_*^{-1/3}$ . The combination of thermal pressure for higher masses and coulomb forces for lower masses conspire to produce  $R_*(M_*) \approx \text{constant}$ . We can model the interior structure — the density distribution — with a function of the form

$$\rho(r) = \rho_c p(\xi) \quad \text{where} \quad \xi = \frac{r}{R_*}, \quad (\text{C.1})$$

and where  $\rho_c$  is the central density. It is convenient to define dimensionless integrals of the form

$$I_k \equiv \int_0^1 p^k \xi^2 d\xi. \quad (\text{C.2})$$

With these definitions, the stellar mass is given by the expression

$$M_* = 4\pi R_*^3 \rho_c I_1, \quad (\text{C.3})$$

where  $I_1$  is of order unity. The stellar luminosity arising from nuclear reactions depends on the power generated per unit volume  $\varepsilon$ , i.e., the luminosity density. For a given nuclear reaction, this quantity can be written in the form

$$\varepsilon(r) = \Gamma \rho^2 \Phi^2 \exp[-\Phi], \quad (\text{C.4})$$

where the composite variable  $\Phi$  is defined by equation (28). For proton-proton fusion under typical stellar conditions, the constant  $\Gamma_0 \approx 2200 \text{ cm}^5 \text{ s}^{-3} \text{ g}^{-1}$ . In general, with enhanced cross sections for nuclear burning, we write the factor in the form  $\Gamma = X\Gamma_0$ , where  $X$  is the enhancement factor.

For these partially degenerate stars, radiative transport through the stellar interior is efficient. As a result, most of the stellar volume attains a single temperature, denoted here as  $T_c$ . In the absence of electron screening (considered below), the total luminosity is given by the expression

$$L_* = \Gamma 4\pi R_*^3 \rho_c^2 \Phi^2 \exp[-\Phi] I_2, \quad (\text{C.5})$$

where the dimensionless integral  $I_2$  is defined through equation (C.2). If we combine the above results, this baseline luminosity can be written in the form

$$L_* = X\Gamma_0 \frac{M_*^2}{4\pi R_*^3} \frac{I_2}{I_1^2} \Phi^2 \exp[-\Phi], \quad (\text{C.6})$$

which can be evaluated to obtain

$$L_* \approx (3L_\odot) X \left( \frac{M_*}{M_J} \right)^2 \left( \frac{R_*}{R_J} \right)^{-3} \Phi^2 \exp[-\Phi]. \quad (\text{C.7})$$

At the high density and relatively low temperatures of degenerate stellar interiors, electron screening can be important. Following classic treatments [54, 55], we define a screening parameter

$$\Lambda = (4\pi n_e)^{1/2} \left( \frac{e^2}{kT} \right)^{3/2}. \quad (\text{C.8})$$

Because of the screening effect, the Coulomb suppression of nuclear reactions is smaller, so that the reactions rates are enhanced. The enhancement factor can be written in the form

$$f = \exp[h(\Lambda)], \quad (\text{C.9})$$

where calculation of the function  $h$  is complicated. In the regime of strong screening, which is applicable to the degenerate low-mass stars of interest, the screening function can be fit with the simple form

$$h = 0.836\Lambda^{2/3} - 0.19. \quad (\text{C.10})$$

The enhancement factor competes with the Coulomb repulsion term and allows nuclear reactions to take place at lower temperatures. The combination of these two effects takes the form

$$\begin{aligned} \Phi^2 \exp[-\Phi] f &= \Phi^2 \exp[-\Phi + h(\Lambda)] \\ &= 7.44 \left( \frac{E_G}{4kT} \right)^{2/3} \exp \left[ 0.836 (4\pi n_e)^{1/3} \left( \frac{e^2}{kT} \right) - 3 \left( \frac{E_G}{4kT} \right)^{1/3} \right]. \end{aligned} \quad (\text{C.11})$$

The star reaches a long-term steady-state configuration when the luminosity generated by nuclear fusion can compensate for the energy lost by cooling. As noted previously, these objects have a nearly degenerate configuration with efficient energy transport, so that most of the stellar volume reaches a single temperature  $T_c$ . The luminosity due to cooling in a degenerate stellar object can be written in the form

$$L_{cool} \sim M^a T_c^b, \quad (\text{C.12})$$

where the power-law indices  $(a, b)$  have been estimated to be  $(1, 7/2)$  for white dwarfs [36] and  $(6/5, 9/2)$  for brown dwarfs [56]. For definiteness, we consider indices  $(1, 4)$  in the following discussion.

If we set the cooling rate (cooling luminosity) equal to the luminosity generated by nuclear reactions, the required value of  $\Phi$  and hence the operating temperature of the star are determined. The value is the given by the solution to an equation of the form

$$(M_*/M_J)X\Phi^{14}\exp[-\Phi + h(\Lambda)] = C. \quad (\text{C.13})$$

The required value of  $\Phi$  thus depends only logarithmically on the stellar mass  $M_*$  and the nuclear enhancement factor  $X$ . As a result, the central temperature  $T_c$  varies slowly with mass. If ones uses the screening factor derived above in conjunction with the luminosity given by equation (C.7), the central temperature  $T_c \sim 10^5$  K leads to the stellar luminosities indicated by the *MESA* simulations for enhancement factor  $X = 10^{15}$ . This central temperature is about an order of magnitude lower than that associated with thermonuclear fusion (e.g, deuterium burning at  $T_c \approx 10^6$  K) and is roughly consistent with the stellar evolution simulations (see Figure 6). Nonetheless, we lack a definitive calculation of the cooling rates, and the luminosity is exponentially sensitive to the temperature  $T_c$ , so this agreement is approximate.

Finally, since these nearly degenerate stars have nearly constant radius, the form of the lower main sequence in the H-R diagram can be readily understood. Using  $R_* = \text{constant}$  in conjunction with the outer boundary condition from equation (44), the stellar luminosity and surface temperature obey the relation  $L_* \sim T_*^4$ . This expression agrees with the slope of the lower main sequence shown in the H-R diagram in Figure 2.

## Appendix D. Stellar Lifetimes versus Enhancement Factor

The stellar evolution simulations in the main text indicate that enhanced cross sections for nuclear reactions result in shorter stellar lifetimes for a given stellar mass, but the range of allowed stellar masses becomes larger. Since the stars with the lowest mass live the longest, these two effects compete. This Appendix considers the balance between these two behaviors. In the limiting case where all stars have access to one and only one nuclear burning reaction, the extension of the mass range dominates, and the stellar lifetime would increase (slowly) with enhancement factor. In more realistic scenarios, however, the smallest stars cannot burn  ${}^3\text{He}$  (into  ${}^4\text{He}$ ) so that their lifetimes are somewhat shorter. As a result, the lifetime of the longest-lived star is always of order trillions of years, nearly independent of the enhancement factor, for the ranges of  $X$  relevant to this paper.

In order to show this dependence on the enhancement factor, we can use the semi-analytic stellar structure model developed earlier [18, 19, 6]. The minimum

stellar mass can be written in the form

$$M_{*\min} = 6(3\pi)^{1/2} \left(\frac{4}{5}\right)^{3/4} \left(\frac{kT_{\text{nuc}}}{m_e c^2}\right)^{3/4} \alpha_G^{-3/2} m_p, \quad (\text{D.1})$$

where  $T_{\text{nuc}}$  is the temperature required for nuclear reactions to take place in the stellar core. In the context of this semi-analytic model, the nuclear burning temperature of the star with the minimum mass is given by the solution to an equation of the form

$$\Phi I(\Phi) = \frac{A}{X}, \quad (\text{D.2})$$

where the quantity  $\Phi$  determines the temperature as defined through equation (28),  $X$  is the enhancement factor, and  $I(\Phi)$  is an integral function of the variable  $\Phi$  [18, 19]. For our universe, the constant  $A$  is given (approximately) by

$$A = N_T \left(\frac{\hbar^3}{c^2}\right) \left(\frac{1}{m_p m_e^3}\right) \left(\frac{G}{\kappa_0 \mathcal{C}}\right), \quad (\text{D.3})$$

where  $N_T$  is a dimensionless constant,  $\kappa_0$  is a fiducial value of the stellar opacity, and  $\mathcal{C}$  sets the nuclear reaction rate. Using the same stellar model, the stellar lifetime has the form

$$t_* = N_* \hbar^3 c^4 \kappa_0 \Phi M_*^{-2} (G m_p)^{-4} \propto \Phi^{11/2}, \quad (\text{D.4})$$

where  $N_*$  is another dimensionless constant. As the enhancement factor  $X$  increases, the required value of  $\Phi$  from equation (D.2) increases, which corresponds to decreasing values of the nuclear burning temperature. As a result, the stellar lifetime of the minimum mass star is predicted to increase as the enhancement factor  $X$  grows larger.

However, the dependence of the lifetime  $t_*(X)$  on the enhancement factor is logarithmic: The integral function in equation (D.2) can be fit with the approximate form so that the expression becomes

$$\Phi^{2.3} \exp[-\Phi] = \frac{A_f}{X}. \quad (\text{D.5})$$

To leading order, we find that  $\Phi \sim \Phi_0 + \ln X$ , where  $\Phi_0 \approx 38$  is the value for the smallest stars in our universe (see [35] and Section 3.1). As a result, the nuclear burning temperature is a slowly decreasing function of the enhancement factor  $X$ , and the stellar lifetime scales according to  $t_* \sim (\Phi_0 + \ln X)^{11/2}$ .

It is important to keep in mind that the semi-analytic model used here does not take into account several complications. First, it assumes only a single nuclear burning species. As found in this paper, however, the lowest mass stars, with

large enhancement factors  $X$ , can burn their protons into  ${}^3\text{He}$ , but are not massive enough for the core to produce  ${}^4\text{He}$ . The lower energy yield (for  ${}^3\text{He}$  versus  ${}^4\text{He}$ ) leads to a lower efficiency of energy conversion and a somewhat shorter lifetime. This correction largely compensates for the logarithmic increase, thereby leading to maximum stellar lifetimes that are roughly constant with  $X$ . Significantly, however, these maximum stellar lifetimes are still measured in trillions of years.

## References

- [1] G.F.R. Ellis, U. Kirchner, and W. R. Stoeger, *Multiverses and Physical Cosmology*, *Mon. Not. R. Astron. Soc.* **347** (2004) 921
- [2] P.C.W. Davies, *Multiverse Cosmological Models*, *Modern Phys. Lett.* **19** (2004) 727
- [3] J. Garriga and A. Vilenkin, *Prediction and Explanation in the Multiverse*, *Phys. Rev. D* **77** (2008) 043526
- [4] L. J. Hall and Y. Nomura, *Evidence for the Multiverse in the Standard Model and Beyond*, *Phys. Rev. D* **78** (2008) 5001
- [5] A. D. Linde, *A Brief History of the Multiverse*, *Ref. Prog. Phys.* **80** (2017) 022001
- [6] F. C. Adams, *The Degree of Fine-Tuning in our Universe — and Others*, *Physics Reports* **807** (2019) 1
- [7] F. J. Dyson, *Energy in the Universe*, *Sci. Amer.* **225** (1971) 50
- [8] P.C.W. Davies, *Time Variation of the Coupling Constants*, *J. Phys. A* **5** (1972) 1296
- [9] J. D. Barrow and F. J. Tipler, *The Anthropic Cosmological Principle*, Oxford Univ. Press (1986)
- [10] T. Pochet, J. M. Pearson, G. Beaudet, and H. Reeves, *The Binding of Light Nuclei, and the Anthropic Principle*, *Astron. Astrophys.* **243** (1991) 1
- [11] M. Tegmark, *Is “The Theory of Everything” Merely the Ultimate Ensemble Theory?* *Annals Phys.* **270** (1998) 1
- [12] C. J. Hogan, *Why the Universe is Just So*, *Rev. Mod. Phys.* **72** (2000) 1149
- [13] M. J. Rees, *Just Six Numbers*, Basic Books (2000)

- [14] T. Dent and M. Fairbairn, *Time-varying Coupling Strengths, Nuclear Forces and Unification*, *Nuc. Phys. B* **653** (2003) 256
- [15] M. Tegmark, A. Aguirre, M. J. Rees, and F. Wilczek, *Dimensionless Constants, Cosmology, and other Dark Matters*, *Phys. Rev. D* **73** (2006) 3505
- [16] A. N. Schellekens, *Life at the Interface of Particle Physics and String Theory*, *Rev. Mod. Phys.* **85** (2013) 149
- [17] J. F. Donoghue, *The Multiverse and Particle Physics*, *Ann. Rev. Nucl. Part. Sci* **66** (2016) 1
- [18] F. C. Adams, *Stars in other Universes: Stellar structure with different fundamental constants*, *J. Cosmol. Astropart. Phys.* **08** (2008) 010
- [19] F. C. Adams, *Constraints on Alternate Universes: Stars and habitable planets with different fundamental constants*, *J. Cosmol. Astropart. Phys.* **02** (2016) 042
- [20] L. A. Barnes, *Binding the Diproton in Stars: Anthropic Limits on the Strength of Gravity*, *J. Cosmol. Astropart. Phys.* **12** (2015) 050
- [21] R.A.W. Bradford, *The Effect of Hypothetical Diproton Stability on the Universe*, *J. Astrophys. Astron.* **30** (2009) 119
- [22] J. MacDonald and D. J. Mullan, *Big Bang Nucleosynthesis: The strong nuclear force meets the weak anthropic principle*, *Phys. Rev. D* **80** (2009) 043507
- [23] J. P. Kneller and G. C. McLaughlin, *Effect of Bound Dineutrons upon Big Bang Nucleosynthesis*, *Phys. Rev. D* **70** (2004) 043512
- [24] D. Lee, U.-G. Meißner, K. A. Olive, M. Shifman, and T. Vonk,  *$\theta$ -Dependence of Light Nuclei and Nucleosynthesis*, arXiv:2006.12321 (2020)
- [25] R. Harnik, G. D. Kribs, and G. Perez, *A Universe Without Weak Interactions*, *Phys. Rev. D* **74** (2006) 035006
- [26] E. Grohs, A. R. Howe, and F. C. Adams, *Universes without the Weak Force: Astrophysical Processes with Stable Neutrons*, *Phys. Rev. D* **97** (2018) 3003
- [27] A. R. Howe, E. Grohs, and F. C. Adams, *Nuclear Processes in Other Universes: Varying the strength of the weak force*, *Phys. Rev. D* **98** (2018) 3014

- [28] B. Paxton, L. Bildsten, A. Dotter, F. Herwig, P. Lesaffre, and F. X. Timmes, *Modules for Experiments in Stellar Astrophysics (MESA)*, *Astrophys. J. Suppl.* **192** (2011) 3
- [29] B. Paxton, M. Cantiello, P. Arras, L. Bildsten, E. F. Brown, A. Dotter, C. Mankovich, M. H. Montgomery, D. Stello, F. X. Timmes, and R. Townsend, *Modules for Experiments in Stellar Astrophysics (MESA): Planets, Oscillations, Rotation, and Massive Stars*, *Astrophys. J. Suppl.* **208** (2013) 4
- [30] E. M. Burbidge, G. R. Burbidge, W. A. Fowler, and F. Hoyle, *Synthesis of the Elements in Stars*, *Rev. Mod. Phys.* **29** (1957) 547
- [31] E. Grohs and G. M. Fuller, *Insights into Neutrino Decoupling Gleaned from Considerations of the Role of Electron Mass*, *Nuclear Physics B* **923** (2017) 222
- [32] E. Grohs, G. M. Fuller, C. T. Kishimoto, and M. W. Paris, *Probing Neutrino Physics with a Self-Consistent Treatment of the Weak Decoupling, Nucleosynthesis, and Photon Decoupling Epochs*, *J. Cosmol. Astropart. Phys.* **5** (2015) 017
- [33] D. D. Clayton, *Principles of Stellar Evolution and Nucleosynthesis*, Univ. Chicago Press (1983)
- [34] R. Kippenhahn and A. Weigert, *Stellar Structure and Evolution*, Springer (1990)
- [35] A. C. Phillips, *The Physics of Stars*, Wiley (1994)
- [36] C. J. Hansen and S. D. Kawaler, *Stellar Interiors: Physical Principles, Structure, and Evolution*, Springer (1994)
- [37] G. M. Fuller, W. A. Fowler, and M. J. Newman, *Stellar Weak-Interaction Rates for sd-Shell Nuclei. I. Nuclear matrix element systematics with application to Al-26 and selected nuclei of importance to the supernova problem*, *Astrophys. J. Suppl.* **42** (1980) 447
- [38] G. M. Fuller, W. A. Fowler, and M. J. Newman, *Stellar Weak Interaction Rates for Intermediate-Mass Nuclei. II.  $A = 21$  to  $A = 60$* , *Astrophys. J.* **252** (1982) 715
- [39] A. Sommerfeld, *Über die Beugung und Bremsung der Elektronen*, *Annalen der Physik* **403** (1931) 257

- [40] E. W. Kolb and M. S. Turner, *The Early Universe*, Addison-Wesley (1990)
- [41] C. Hayashi, *Stellar Evolution in Early Phases of Gravitational Contraction*, *Pub. Astron. Soc. Japan* **13** (1961) 450
- [42] G. Laughlin, P. Bodenheimer, and F. C. Adams, *The End of the Main-Sequence*, *Astrophys. J.* **482** (1997) 420
- [43] F. Adams and G. Laughlin, *A Dying Universe: The long term fate and evolution of astrophysical objects*, *Rev. Mod. Phys.* **69** (1997) 337
- [44] F. C. Adams and M. Fatuzzo, *A Theory of the Initial Mass Function for Star Formation in Molecular Clouds*, *Astrophys. J.* **464** (1996) 256
- [45] A. S. Grossman and H. C. Graboske, *Evolution of Low-Mass Stars. V: Minimum mass for the deuterium main sequence*, *Astrophys. J.* **180** (1973) 195
- [46] U.-G. Meißner, *The Long and Winding Road from Chiral Effective Lagrangians to Nuclear Structure*, *Physica Scripta* **91** (2016) 3005
- [47] F. C. Adams and E. Grohs, *Stellar Helium Burning in Other Universes: A solution to the triple alpha fine-tuning problem*, *Astropart. Phys.* **87** (2017) 40
- [48] L. Huang, F. C. Adams, and E. Grohs, *Sensitivity of Carbon and Oxygen Yields to the Triple-Alpha Resonance in Massive Stars*, *Astropart. Phys.* **105** (2019) 13
- [49] M. Livio, D. Hollowell, J. M. Truran, and A. Weiss, *The Anthropic Significance of the Existence of an Excited State of C-12*, *Nature* **340** (1989) 281
- [50] H. Schlattl, A. Heger, H. Oberhummer, T. Rauscher, and A. Csótó, *Sensitivity of the C and O Production on the  $3\alpha$  Rate*, *Astrophys. Space Sci.* **291** (2004) 27
- [51] E. Epelbaum, H. Krebs, T. A. Lähde, D. Lee, and U.-G. Meißner, *Dependence of the Triple-alpha Process on the Fundamental Constants of Nature*, *Eur. Phys. J. A* **49** (2013) 82
- [52] F. C. Adams and E. Grohs, *On the Habitability of Universes without Stable Deuterium*, *Astropart. Phys.* **91** (2017) 90
- [53] L. A. Barnes and G. F. Lewis, *Producing the Deuteron in Stars: Anthropic limits on fundamental constants*, *J. Cosmol. Astropart. Phys.* **07** (2017) 036

- [54] H. E. DeWitt, H. C. Graboske, and M. S. Cooper, *Screening Factors for Nuclear Reactions. I. General theory*, *Astrophys. J.* **181** (1973) 439
- [55] H. C. Graboske, H. E. DeWitt, A. S. Grossman, and M. S. Cooper, *Screening Factors for Nuclear Reactions. II. Intermediate screening and astrophysical applications*, *Astrophys. J.* **181** (1973) 457
- [56] S. Auddy, S. Basu, and S. R. Valluri, *Analytic Models of Brown Dwarfs and the Substellar Mass Limit*, *Adv. Astrophys.* **16** (2018) 13